Online Materials for:

Neurospora chromosomes are organized by blocks of importin alpha-dependent heterochromatin that are largely independent of H3K9me3

Jonathan M. Galazka[1†*], Andrew D. Klocko[2*], Miki Uesaka[3], Shinji Honda[3], Eric U. Selker[2], and Michael Freitag[1‡]

[1]Department of Biochemistry and Biophysics, Oregon State University, Corvallis, OR 97331

[2]Institute of Molecular Biology, University of Oregon, Eugene, OR 97403

[3]Department of Biochemistry and Bioinformative Sciences, Faculty of Medical Sciences, University of Fukui, Fukui, Japan

[†]Present address: Space Biosciences Division, NASA Ames Research Center, Moffett Field, CA 94035

*These authors contributed equally to this work.

[‡]Corresponding Author: Michael Freitag

2011 ALS Bldg, Department of Biochemistry and Biophysics, Oregon State University, Corvallis, OR 97331

Email: freitagm@cgrb.oregonstate.edu. Phone: (541) 737-4845

List of Supplemental Materials

Supplemental Materials and Methods

Culture conditions, crosslinking and spheroplasting.

Duplicate 50 mL cultures were inoculated with $2.5x10^8$ conidia and grown at 30°C with shaking at 200 revolutions per minute (RPM). After germination (~3-4 hrs), 2.6 mL of methanol-free formaldehyde (20%) was added to a final concentration of 1%. After 10 min incubation at room temperature (RT) with shaking at 100 RPM, crosslinking was quenched by adding 3.4 mL of 2 M Tris-HCl [pH 8 at 25°C] to a final concentration of 125 mM and incubated at RT for another 10 min with shaking at 100 RPM. Conidia were harvested by centrifugation (3000 RPM, 5 min) and resuspended gently in 40 mL spheroplasting buffer (1 M sorbitol, 100 mM KPO_4 [pH 7.5]) plus 30 mM β-mercaptoethanol, pelleted again and resuspended in 40 mL spheroplasting buffer. VinoTaste Pro (Novozymes; 200 mg) was added and strains were spheroplasted for 60 min at 30°C with shaking at 100 RPM. Spheroplasts were harvested by centrifugation (2000 RPM, 5 min) and washed three times with 20 mL HindIII buffer (50 mM NaCl, 10 mM Tris-HCl [pH 7.9 at 25°C], 10 mM $MgCl_2$, 100 μg/mL bovine serum albumin [BSA]). Washed pellets were resuspended in 6 mL

HindIII buffer, split into 1 mL aliquots in 1.7 mL Eppendorf tubes. Spheroplasts were pelleted (1500 g, 5 min) and the supernatant was aspirated away. Aliquots were frozen in liquid nitrogen and stored at -80°C.

Hi-C and 3C library construction

Hi-C libraries were produced as previously described (Lieberman-Aiden et al. 2009). Unless otherwise stated, enzymes were purchased from New England Biolabs (NEB).To determine the concentration of genomic DNA (gDNA) per aliquot of spheroplasts, 1 aliquot per replicate was resuspended in 200 µL decrosslinking buffer (50 mM Tris-HCl [pH 8], 5 mM Na ethylenediaminetetraacetic acid [Na EDTA], 0.5% [w/v] sodium dodecyl sulfate [SDS]) plus 100 mg proteinase K (Invitrogen) and incubated at 65°C overnight. The next day, the volume was brought to 500 µL with TE buffer (10 mM Tris-HCl [pH 8], 1 mM Na-EDTA) plus 40 mg RNase A (Invitrogen) and aliquots were incubated at 37°C for 30 min. gDNA was then extracted twice with a 1:1 mixture of buffered phenol (pH 8) and chloroform, and once with chloroform. gDNA was precipitated by adding 1/10 volume of Na acetate (pH 5.2) and 1 volume of isopropanol. DNA pellets were washed three times with 70% (v/v) ethanol, dried at RT for 10 min and resuspended in 50 µL TE. The DNA concentration was estimated from the absorbance at 260 nm.

Spheroplasts corresponding to 3.5 µg of gDNA were resuspended in 270 µL of HindIII buffer and 30 µL of 10% (w/v) SDS was added to a final concentration of 0.1% (w/v). Spheroplasts were then lightly decrosslinked by incubation at 65°C for 10 min and placed immediately on ice. 33 µL of 10% (v/v) Triton X-100 and 8.3 µL of 10x HindIII buffer was added and gDNA digested with 400 U (20 µL of 20 U/µL from NEB) HindIII for 16 hrs at

37°C while mixing. The next day, samples were placed on ice and split into two aliquots.

To construct Hi-C libraries, one aliquot of HindIII digested chromatin was labeled with biotin-14-dCTP (Invitrogen) in a 210 µL reaction consisting of 30 µM dATP, 30 µM dTTP, 30 µM dGTP, 30 µM biotin-14-dCTP and 25 U of Klenow (large fragment). This reaction was incubated at 37°C for 45 min with nutating. Enzymes were inactivated by the addition of SDS to 1.5% (w/v) and incubation at 65°C for 30 min. This chromatin was then used in a 3.5 mL ligation reaction consisting of 50 mM Tris-HCl [pH 7.5 at 25°C], 10 mM $MgCl_2$, 0.9% (v/v) Triton X-100, 10 mM dithiothreitol (DTT), 100 µg/mL BSA, 1 mM ATP and 1,675 U T4 DNA ligase (4.2 µL of 400,000 U/mL T4 DNA ligase). This reaction was incubated at 16°C for 4 hrs.

At the end of the 4-hour 3C and Hi-C ligation reactions, 250 mg of proteinase K (Invitrogen) was added and all reactions were allowed to decrosslink at 65°C overnight. The next day, another 250 mg of proteinase K was added and samples were decrosslinked at 65°C for another 2 hrs. Samples were cooled to ~25°C on ice, and extracted with 5 mL of phenol (pH 8) by vortexing for 2 min. After centrifugation, the aqueous phase was removed and extracted with 5 mL of phenol (pH 8):chloroform (1:1) by vortexing for 2 min. After centrifugation, the aqueous phase was removed and brought to a volume of 5 mL with TE. DNA was precipitated by the addition of 0.5 mL 3 M Na-acetate [pH 5.2], 50 mg glycogen, 12.5 mL 95% ethanol and incubation at -80°C for 1 hr. DNA was pelleted by centrifugation (20,000 g, 20 min), the supernatant decanted and DNA resuspended in 450 µL TE by vortexing. DNA was again extracted with 1 volume of phenol (pH 8):chloroform (1:1) and then chloroform as before. DNA was ethanol precipitated as before and resuspended in 25 µL of TE/10 buffer (10 mM Tris-HCl [pH 8 at 25° C], 0.1 mM Na-EDTA).

To remove biotin-dCTP from unligated ends, the Hi-C libraries were digested for 2 hrs at 12°C in a 50 µL reaction consisting of 5 µL of NEB buffer 2, 100 µg/mL BSA, 100 µM dATP, 100 µM dGTP and 5 U of T4 DNA polymerase. These reactions were quenched by adding Na-EDTA to 10 mM and DNA extracted with 1 volume of phenol (pH 8):chloroform and then with 1 volume of chloroform. DNA was ethanol precipitated, resuspended in 500 µL of TE and sheared by sonication (duty cycle 80, power 1.2, 10 s, 5x with 1 minute rest on ice between pulses). Sheared, biotinylated DNA was captured by adding 25 µL of streptavidin magnetic beads (Invitrogen) that had been equilibrated in BW buffer (5 mM Tris-HCl [pH 8 at 25°C], 0.5 mM Na-EDTA, 1 M NaCl, 0.05% [v/v] Tween-20), and incubating for 30 min with shaking. Beads were washed 2x with BW buffer, 2x with TE/10 buffer (10mM Tris-HCl pH 8.0, 0.1mM EDTA) and resuspended in 25 µL TE/10 buffer. Library preparation was performed with DNA fragments attached to magnetic-beads with repeated washes and reagent changes, up to the final PCR step.

To prepare Hi-C libraries for Illumina sequencing, either Illumina TruSeq kits were used according to the manufacturer's protocol, or replaced by an improved version of that protocol. For this, DNA ends were repaired in reactions consisting of 25 µL of Hi-C libraries on streptavidin beads, 5 µL of T4 DNA ligase buffer, 2 µL 10 mM of each dNTPs, 0.5 µL end repair enzyme mix (0.5 U T4 DNA polymerase, 0.25 U Klenow [large fragment], 2.25 U T4 DNA polynucleotide kinase) in a final volume of 50 µL and incubated at 20°C for 30 min. Beads were washed twice with BW buffer and twice with TE/10, and resuspended in 16.5 µL TE/10. A-tailing was performed by adding 2 µL 10x NEB Buffer #2, 1 µL 4 mM dATP, 0.5 µL Klenow 3' to 5' exo minus (5 U/µL) and incubating at 37 C for 30 min, mixing every 10 min. Beads were again washed with BW and TE/10 buffers as above and resuspended in 20

μL TE/10. Indexed adaptors were ligated by adding 25 μL 2x ligase buffer (132 mM Tris-HCl [pH 7.6], 20 mM $MgCl_2$, 2 mM DTT, 2 mM ATP, 15% [w/v] PEG 6000), 2.5 μL T4 DNA ligase (400 U/μL) and 2.5 μL Illumina TruSeq DNA adapters diluted 1:10 and incubating at RT for 20 min, mixing every 10 min. Ligation reactions were quenched with 5 μL of 0.5 M Na-EDTA (pH 8) and beads washed three times with BW buffer and twice with TE/10. Beads were then resuspended in 50 μL TE/10 and Hi-C libraries amplified in 50 μL PCR reactions using Phusion polymerase (Thermo-Fisher or NEB) and the following cycle: 45 s at 98°C; 18 cycles of 15 s at 98°C, 30 s at 63°C, 30 s at 72°C; 1 min at 72°C. The PCR product was separated from the beads, cleaned with Ampure XP beads (Agencourt, Beckman-Coulter) according to the manufacturer's instructions, and resuspended in 25 μL TE/10. Library quality was assessed by gel electrophoresis before sequencing.

Deconvolution Microscopy and Nuclear Membrane Distance Analysis

Conidia resuspended in 50% glycerol were imaged on an Olympus IX71 DeltaVision microscope using a 60x, 1.42 numerical aperture objective (Olympus) with the 1.6x "optibar" engaged (final resolution = 96x). 3D Z-stack wide-field images were captured with the DeltaVision softWoRx (GE Healthcare, version 6.5.2) software using FITC (GFP) and DAPI (BFP) filters, and subjected to 15 iterations of "conservative ratio" deconvolution.

Closest distances (often between Z-stacks) from the TRF-1-GFP (telomere) center to the ISH-1-BFP (nuclear membrane; NM) center were measured in 3D using DeltaVision softWoRx software; telomeres directly contacting the NM were assigned the shortest measurable distance (0.109 μm, a single pixel). NM diameter was measured in two different directions in the Z stack where the NM appeared largest, and the average NM

diameter was used for calculations. Boxplot of NM diameter, and its associated variance statistics (ANOVA test), were generated in Rstudio. Telomere foci zone assignment performed as in (Meister et al. 2010), where telomere-NM distance was divided by the NM radius (r), and placed into one of three zones based on Zone radii (<0.184 x r for Zone 1, >0.184 x r to <0.422 x r for Zone 2, >0.422 x r for Zone 3; all zone radii are thus are normalized to the NM size; Taddei et al. 2004; 2006; Hediger et al. 2002; Meister et al. 2010). ISH-1-BFP signal was false colored red, and a single Z stack images were used for Fig. 5.

Supplemental References

Hediger F, Neumann FR, Van Houwe G, Dubrana K, Gasser SM. 2002. Live imaging of telomeres: yKu and Sir proteins define redundant telomere-anchoring pathways in yeast. *Curr Biol* **12**: 2076–89.

Lieberman-Aiden E, van Berkum NL, Williams L, Imakaev M, Ragoczy T, Telling A, Amit I, Lajoie BR, Sabo PJ, Dorschner MO, et al. 2009. Comprehensive mapping of long-range interactions reveals folding principles of the human genome. *Science* **326**: 289–93.

Meister P, Gehlen LR, Varela E, Kalck V, Gasser SM. 2010. Visualizing Yeast Chromosomes and Nuclear Architecture. *Methods in Enzymology* **470**: 535–67.

Smith KM, Phatale PA, Sullivan CM, Pomraning KR, Freitag M. 2011. Heterochromatin is required for normal distribution of *Neurospora crassa* CenH3. *Mol Cell Biol* **31**: 2528–42.

Taddei A, Hediger F, Neumann FR, Bauer C, Gasser SM. 2004. Separation of silencing from perinuclear anchoring functions in yeast Ku80, Sir4 and Esc1 proteins. *EMBO J* **23**: 1301–12.

Taddei A, Van Houwe G, Hediger F, Kalck V, Cubizolles F, Schober H. 2006. Nuclear pore association confers optimal expression levels for an inducible yeast gene. *Nature* **441**: 774–8.

Supplemental Table S1. Strains used and DNA sequencing datasets obtained.

For each dataset, the strain number, genotype, read length in nucleotides, number of raw read pairs, and number of read pairs passing all quality control filters are shown.

Dataset	Strain	Genotype	Read length	Raw reads	Read pairs passing filters
WT rep1	NMF39	*mat A*	100 nt	15,884,233	621,218
WT rep2	NMF39	*mat A*	50 nt	23,452,879	3,085,113
WT rep3	NMF39	*mat A*	50 nt	21,867,121	3,612,235
Δ*dim-5* rep1	N3944	*mat A*; *Δdim-5::bar*	50 nt	22,049,495	2,909,026
Δ*dim-5* rep2	N3944	*mat A*; *Δdim-5::bar*	50 nt	22,837,712	2,334,710
Δ*hpo* rep1	N5580	*mat a*; *Δhpo::hph; his-3*	50 nt	21,728,811	1,793,646
Δ*hpo* rep2	N5580	*mat a*; *Δhpo::hph; his-3*	50 nt	22,004,120	2,159,249
dim-3 rep1	N2108	*mat A*; *dim-3*	50 nt	22,591,516	743,441
dim-3 rep2	N2108	*mat A*; *dim-3*	75 nt	19,863,212	1,414,434

Supplemental Figure Legends

Supplemental Fig. S1. Data coverage of the WT Hi-C heatmap drops as resolution is increased.

A binary heatmap of the entire *N. crassa* genome is shown at six different resolutions, produced by the script binaryCoverage.py. Black pixels indicate regions that were observed interacting at least once, while white pixels indicate that those regions were not observed to interact. Coverage of rare long-range interactions drops as resolution is increased, while frequency of local interactions and strong heterochromatin interactions remain well sampled down to a resolution of 10 kb.

Supplemental Fig. S2. Data coverage of the WT Hi-C heatmap increases slowly as read number is increased.

[A] Plot showing the percentage of possible interactions *not* observed in the merged WT Hi-C dataset as resolution is decreased from 10 kb to 110 kb, produced by the script binsWithoutDataRes.py. [B] Plot showing the percent of possible interactions observed in the merged WT Hi-C dataset as read number is increased from 5 to 50 million when datasets are sampled at resolutions of 10 kb (inverted open triangles), 20 kb (black triangles), 30 kb (open triangles), 40 kb (closed circles) or 50 kb (open circles), produced by the script binsWithoutDataReads.py.

Supplemental Fig. S3. Data coverage is sufficient to assay local contacts at 10 kb and median contact frequency in the *dim-3* dataset decays more slowly than WT.

[A] Plot showing the percentage of genomic regions covered with at least 1000

observations as resolution is decreased in WT, Δ*dim-5*, Δ*hpo* and *dim-3* strains, produced by script binsWith1000.py. [B] Log_{10}-log_{10} plot of observed contact probabilities *vs*. genomic distance for WT, Δ*dim-5*, Δ*hpo* and *dim-3* strains, produced by the script HiCScaling.py.

Supplemental Fig. S4. Hi-C reveals an inversion of LGVI in Assembly 12 of the *N. crassa* genome.

[A] Schematic of the contigs comprising LGVI in Assembly 12 of the *N. crassa* genome. Breaks between contigs are denoted with vertical lines. Contig_12.304 is colored pink and begins and ends in A:T-rich heterochromatic regions. Levels of CenH3 (ChIP-seq data; (Smith et al. 2011) and H3K9me3 enrichment are shown as histograms below the schematic. [B] An alignment of assemblies 10 and 12 of *N. crassa* LGVI showing a large inverted region corresponding to Contig_12.304. Analysis was done with the program MUMmer (http://mummer.sourceforge.net/). [C] Heatmaps of observed contact frequencies before (left) and after (right) flipping the orientation of Contig_12.304.

Supplemental Fig. S5. WT Hi-C datasets are highly reproducible.

[A] Heatmaps of observed contact frequencies in LGII from two biological replicates of WT *N. crassa* at 40 kb resolution are shown as examples. Similar results were obtained with all chromosomes. [B] A log_{10}-log_{10} plot of the observed probability of contact *vs*. genomic distance for two biological replicates of WT *N. crassa* (red and blue lines), generated by the script HiCScaling.py, revealed almost completely overlapping curves. [C] Heatmap of

observed contact frequencies in LGII after combing the two WT replicates in [A].

Supplemental Fig. S6. Method for dataset normalization and calculating expected contact frequency matrix.

[A] Heatmap of observed contact frequencies in LGII of WT *N. crassa* at 20 kb resolution after normalizing for sequencing depth (dividing each contact frequency by the mean contact frequency). [B] Plots of the median contact frequency *vs*. genomic distance for all strains before (left plot) and after (right plot) normalization performed in A, produced by the script observedExpectedMethod.py. Note the smaller differences between the datasets following normalization. [C] Plot of instantaneous slopes from the normalized plot in B, produced by the script observedExpectedMethod.py. The inset shows an expanded view of the larger plot. The vertical line at ~2.5 Mb indicates the point at which the median number of contacts stops decreasing with genomic distance. [D] Heatmap showing matrix of expected contact frequencies for LGII produced by calculating the median contact frequency at each genomic distance less than 2.5 Mb, at which point the contact frequency had reached background. [E] Heatmap showing the ratio (log_2) of observed contacts *vs.* expected contacts produced by dividing the normalized observed matrix in A with the expected matrix in D.

Supplemental Fig. S7. WT change from expected contact frequencies.

Whole genome heatmap plotting the ratio (log_2) of the observed contact frequency *vs.* the expected (median) genomic distance frequency at 40 kb resolution. The seven

chromosomes (LGI - LGVII) are shown as elongated ovals with the approximate centromere locations indicated as green bars. Regions with greater than expected contact frequencies are shown in red hues. Examples include inter-chromosomal contacts between the seven centromeres and the 14 subtelomeres. Regions with less than expected contact frequencies are shown in blue hues. Examples include the infrequent contacts observed between centromeres and chromosome arms. Note that the signal for strong local interactions (the red diagonal evident in Fig. 1A) is no longer dominant after normalization with expected contact frequencies.

Supplemental Fig. S8. The extent of the centromere regions are minimally changed in Δ*dim-5* and Δ*hpo* strains.

[A] The strong signal for reduced contacts between centromeres and chromosome arms in Hi-C datasets (with replicates combined) was used to estimate the extent of centromeres. For each centromere, the observed *vs*. expected values of each bin ~100 kb to either side of the centromere core were plotted together. Lines 1 and 2 in panel B (right) correspond to lines numbered 1 and 2 and represent two independent "cross-sections" or "transects" of the centromere and neighboring regions. The distance of these transects from the centromeres (~100 kb) was selected to best capture the boundaries seen in Hi-C datasets. Other distances give similar results. In these plots, the "U-shaped" drops in the observed *vs*. expected values correspond to the isolation of centromeres from the chromosome arms. The extent of this signal was determined by measuring the width of the "U" at an observed *vs*. expected value of 1.5 (solid horizontal line shows this for WT). Centromere extents in Δ*dim-5* and Δ*hpo* were determined in the same way. The LGI dataset was relatively noisy

and thus was not included in this analysis. [B] The left panel shows the WT LGII Hi-C heatmap (combined replicates) at 10 kb resolution, the boxed region of which is expanded in the right panel. The black lines indicate the bins that were extracted for the line plot in panel A. Lines 1 and 2 in B correspond to lines 1 and 2 in A, respectively. [C] Scatterplot showing centromere extents calculated from the WT Hi-C dataset (panel A) *vs*. the extents determined by ChIP-sequencing of the centromeric histone H3 variant, CenH3 (Smith et al. 2011). The dashed line represents a perfect correlation of 1.0. [D] Plot of centromere extents measured from Hi-C datasets (panel A) for WT, Δ*dim-5*, and Δ*hpo* strains.

Supplemental Fig. S9. Heterochromatic regions flanking the WT pericentromere interact to isolate the centromere.

[A] (Top) Triangular heatmap (one half of a standard square heatmap divided at the strong diagonal and rotated by 45°) of observed contact frequencies at 10 kb resolution around the centromere of LGVII. (Below) The three tracks aligned to the heatmap display CenH3 enrichment, DNA density in each 10 kb region, and accessibility of each region to a 75 nm diameter sphere ("particle"). The density and accessibility values were determined from three-dimensional models shown in B. [B] Three views of a 3D chromatin model within a 1.1 Mb region (1.7 - 2.8 Mb) of LGVII that includes the ~290 kb centromere and ~60 kb pericentric chromatin (Smith et al. 2011). This three-dimensional model is shown both as a continuous wire, left, and as spheres, right. The path of the wires pass through the center of a series of 10 kb spheres, the relative conformation of which were determined using the contact frequencies in the WT Hi-C dataset to set attractive or repulsive forces between

each sphere and allowing the system to relax to a low energy state. This model was produced using the programs TADbit and IMP as described in the Materials and Methods section but using only Hi-C data from the 1.1 Mb centromeric region shown in the heatmap in [A]. Increasing red color indicates regions enriched with the heterochromatic mark H3K9me3, which overlaps with CenH3 enrichment.

Supplemental Fig. S10. The number of strong intra-chromosomal interactions is sensitive to read number.

[A] Circos plot of strong intra-chromosomal contacts in WT LGII using all available reads (61.2 million). Contacts with a $\log_2$ enrichment value over the expected value ≥2.25 are shown as black links between chromosome regions. Contact frequencies are indicated by variations in line thickness. H3K9me3, CenH3 and H3K27me2/3 enrichment from a WT strain are shown as green, orange and purple histograms, respectively, and genomic distance from the left telomere is indicated around the plot. [B-D] As in [A] but after randomly sampling 42, 30 or 16.5 million reads, respectively, from the WT dataset.

Supplemental Fig. S11. Plots of the strongest intra-chromosomal contacts for all chromosomes at 10 kb resolution.

Circos plots of the strongest intra-chromosomal contacts within all WT chromosomes (LGI-VII) at 10 kb resolution after normalizing for genomic distance. Black links indicate contacts with a $\log_2$ enrichment ≥2.25. Contact frequencies are indicated by variations in line thickness. Enrichment with H3K9me3, CenH3 and H3K27me2/3 in a WT strain are shown as green, orange and purple histograms, respectively. Genomic distance from the left telomere is indicated.

Supplemental Fig. S12. Heterochromatin segregates euchromatic globules.

[A] Larger triangular heatmaps (one half of a square heatmap divided at the strong diagonal and rotated 45°) show the observed contact frequencies for LGII from the indicated strains at 10 kb resolution. Below these heatmaps, from top to bottom, are contact bias plots [where blue indicates that the region makes more contacts with regions toward the right subtelomere ("downstream") than with regions toward the left subtelomere ("upstream") and the reverse for red regions, produced with the script contactBias.py], the output from the TADbit package for detecting topologically associated domains (TADs) [arcs ≥ 1 signify the detection of a TAD], and tracks showing H3K9me3 enrichment, %GC content, and gene locations. The smaller heatmaps (above) and tracks show an expansion of the right arm of LGII indicated with an orange line (3.5 - 4.3 Mb). [B] As in [A], but at 20 kb resolution because the data coverage of the weaker, off diagonal bins in the *dim-3* strain is low at 10 kb resolution.

Supplemental Fig. S13. Observed differences between WT and Δ*dim-5* interactions are robust.

[A] Heatmaps of observed contact frequencies ($\log_2$) for two Δ*dim-5* biological replicates at 40 kb resolution. [B] Heatmaps showing all four combinations of comparisons between two WT and two Δ*dim-5* replicates to demonstrate that observed changes are robust.

Supplemental Fig. S14. Whole genome Hi-C datasets of a Δ*dim-5* strain show changes in interactions between heterochromatic regions.

[A] Heatmap of contact frequencies (log_2) for all seven chromosomes (LGI - LGVII) in a Δ*dim-5* strain at 50 kb resolution. The extent of the chromosomes is denoted with elongated ovals with the centromeres indicated as green bars. [B] Whole genome heatmap plotting the ratio (log_2) of the observed contact frequency *vs.* the expected (median) genomic distance frequency of a Δ*dim-5* strain, as in Supplemental Fig. S7. [C] Whole genome heatmap showing the fold change (log_2) in observed *vs.* expected contact frequencies between Δ*dim-5* and WT strains at 50 kb resolution.

Supplemental Fig. S15. Reduced interactions between heterochromatin flanks in a strain lacking HP1.

[A] Heatmap of observed contacts (log_2) within LGII in a Δ*hpo* strain at 50 kb resolution. [B] Heatmap of LGII showing the ratio (log_2) between the observed frequency of interactions and the median frequency at each genomic distance in a Δ*hpo* strain. [C] Heatmap showing the fold change in contact frequencies (log_2) of LGII between the Δ*hpo* and WT strains. WT levels of H3K9me3 are displayed in green above and to the left, and black arrows highlight decreased pericentromeric flank contacts while the purple arrow marks a decreased interspersed heterochromatic flank region. [D] Heatmaps of the combined observed to expected ratios from all seven centromeres in WT (top) and Δ*hpo* (bottom) strains, produced by the script plotCentromeres.py. [E] Circos plot of the largest changes in inter-chromosomal interaction frequencies between WT and Δ*hpo* strains; the WT dataset contains 30 million sampled reads while the Δ*hpo* dataset contains 49 million sampled reads to ensure equivalent numbers of filtered reads. Regions with increased interaction frequencies are in red, while regions with decreased frequencies are in blue, and

differences in the absolute magnitude of the changes are shown as differences in the line thicknesses. The histograms of H3K9me3 (green), CenH3 (orange), and H3K27me2/3 (purple) histograms are from a WT strain; previous work showed that a Δ*hpo* strain has a reduced extent of CenH3 at centromeres (Smith et al. 2011).

Supplemental Fig. S16. Observed differences between WT and Δ*hpo* strains are robust.

[A] Heatmaps of observed contact frequencies (log_2) for two biological replicates of the Δ*hpo* strain at 40 kb resolution. [B] Heatmaps showing all four combinations of comparisons between two WT and two Δ*hpo* replicates reveal that observed changes are robust.

Supplemental Fig. S17. Whole genome Hi-C dataset from a Δ*hpo* strain shows changes in interactions between heterochromatic regions.

[A] Heatmap of observed contact frequencies (log_2) for all seven chromosomes (LGI - LGVII) in a Δ*hpo* strain at 50 kb resolution. The extent of LGI - LGVII is denoted with elongated ovals with the centromeres indicated as green bars. [B] Whole genome heatmap plotting the ratio (log_2) of the observed contact frequency *vs.* the expected (median) genomic distance frequency of a Δ*hpo* strain, as in Supplemental Fig. S7. [C] Whole genome heatmap showing the fold change (log_2) in observed vs. expected contact frequencies between Δ*hpo* and WT strains.

Supplemental Fig. S18. Contacts between pericentromeres are diminished in heterochromatin mutants.

[A] Heatmaps showing the average observed to expected ratio (log_2) for the sum of all seven centromeres of WT, Δ*dim-5,* Δ*hpo* and *dim-3* strains at 20 kb resolution. Boxes correspond to interactions between pericentromeres. [B] Plot showing the average signal within the boxes in A corresponding to pericentromere interaction strength for two replicates of WT, Δ*dim-5,* Δ*hpo* and *dim-3* strains, produced with the script plotCentromeres.py.

Supplemental Fig. S19. Intra-chromosomal contacts are altered in all three heterochromatin mutants.

[A-C] Circos plot of the largest changes in intra-chromosomal interaction frequencies within two single chromosomes, LGII (left) and LGIII (right) in Δ*dim-5* [A], Δ*hpo* [B], and *dim-3* [C] strains compared to WT. Equivalent numbers of filtered reads were used for each comparison. Regions with increased interaction frequencies are in red, while regions with decreased frequencies are in blue, and the absolute magnitude of the changes are indicated by differences in line thickness.

Supplemental Fig. S20. Decreased inter-subtelomeric interactions in heterochromatin mutants.

[A] Heatmaps displaying the interactions (log_2) between the right subtelomere (y-axis) and the left subtelomere (x-axis) for WT and the Δ*dim-5,* Δ*hpo* and *dim-3* mutant strains. Inter-telomeric contacts are expected in the bottom left box, while nearest neighbor "background" interactions within subtelomeres are expected in the top right box. Figures were produced with the script telomereSignal.py. [B] Fold enrichment of the inter-

subtelomeric contacts (bottom left box) of each Hi-C dataset replicate of each heterochromatin mutant strain over the background signal (top right box) of that strain, produced with the script telomereSignal.py.

Supplemental Fig. S21. The heterochromatin network in a Δ*dim-5* strain.

[A] Circos plot of the strongest intra-chromosomal contacts within LGII at 10 kb resolution after normalizing for genomic distance. Black links indicate contacts with a $\log_2$ enrichment ≥2.25. Contact frequencies are indicated by variations in line thickness. Note absence of intra-chromosomal interactions across the centromere and pericentromeric regions when compared to Fig. 1C. [B] Circos plot of the strongest inter-chromosomal contacts at 10 kb resolution after normalizing for genomic distance. Black links indicate contacts with a $\log_2$ frequency ≥3.0. [C] Plot of frequently observed Δ*dim-5* strain contacts between heterochromatic regions from all seven chromosomes (LGI - LGVII) at 10 kb resolution. Green links indicate frequent contacts between regions enriched with H3K9me3, while purple links indicate frequent contacts between regions enriched with H3K27me2/3. Links inside and outside the plot show inter- and intra-chromosomal associations, respectively.

Supplemental Fig. S22. The heterochromatin network in a Δ*hpo* strain.

[A] Circos plot of the strongest intra-chromosomal contacts within LGII at 10 kb resolution after normalizing for genomic distance. Black links indicate contacts with a $\log_2$ enrichment ≥2.25. Thicker lines indicate more frequent interactions. [B] Plot of the strongest inter-chromosomal contacts at 10 kb resolution. Black links indicate contacts with a $\log_2$ frequency ≥3.75. Thicker lines indicate more frequent interactions. [C] Plot of frequently

observed Δ*hpo* strain contacts between heterochromatic regions from all seven chromosomes (LGI - LGVII) at 10 kb resolution. Green links indicate frequent contacts between regions enriched with H3K9me3, while purple links indicate frequent contacts between regions enriched with H3K27me2/3. Links inside and outside the plot show inter- and intra-chromosomal associations, respectively.

Supplemental Fig. S23. Observed differences between WT and *dim-3* interactions are robust.

[A] Heatmaps of observed contact frequencies (log_2) for two *dim-3* biological replicates at 50 kb resolution. [B] Heatmaps showing all four combinations of comparisons between two WT and two *dim-3* replicates to demonstrate that observed changes are robust. The first replicate showed reduced euchromatic interactions that most likely result from lower sequencing depth. However, all strong interactions (i.e.., inter- and intra-centromeric interactions) have sufficient sequence depth for analysis (no empty bins in regions of centromeres, pericentromeres, subtelomeres, or interspersed heterochromatin). In addition, all trends in chromatin interactions are consistent between the two *dim-3* replicates (e.g., reduced inter-subtelomeric interactions and increased centromere-euchromatin interactions). Thus, we conclude that our *dim-3* replicates are representative of the *dim-3* interactions, allowing for merging of the *dim-3* replicate datasets for subsequent analyses.

Supplemental Fig. S24. Whole genome Hi-C dataset from a *dim-3* mutant reveals changes in interactions between heterochromatic regions.

[A] Heatmap of observed contact frequencies (log_2) for all seven chromosomes (LGI - LGVII) in a *dim-3* strain at 50 kb resolution. The chromosomes (LGI – LGVII) are illustrated as elongated ovals with the centromeres indicated with green bars. [B] Whole genome heatmap plotting the ratio (log_2) of the observed contact frequency *vs.* the expected (median) genomic distance frequency in the *dim-3* strain as in Supplemental Fig. S7. [C] Whole genome heatmap showing the fold change (log_2) in observed vs. expected contact frequencies between *dim-3* and WT strains.

Supplemental Fig. S25. Apparent differences between WT and *dim-3* datasets are more pronounced before normalizing with expected contact frequencies.

[A] (Left) Heatmap comparison of the *dim-3* observed *vs.* expected and WT observed *vs*. expected data for LGII. H3K9me3 ChIP-seq tracks are displayed above and to the left for this and all subsequent heatmaps. (Right) Heatmap comparison of the *dim-3* raw interaction and WT raw interaction datasets for LGII. The apparent decrease in interactions near the diagonal result from consistently reduced contact frequencies at short genomic distances for the *dim-3* dataset, and may be indicative of a genome-wide reduction in local strong interactions (see Fig. 5E). [B] Comparisons as in [A], but for the Δ*dim-5* strain, which does not exhibit the drastic changes seen with the *dim-3* strain.

Supplemental Fig. S26. The *dim-3* strain shows an increase in inter-chromosomal ligation products.

Bar graph displaying the relative abundance of intra-chromosomal (light gray) and inter-chromosomal (dark gray) ligation products within the dataset of each strain, produced

with the script 02_filterBatch.py. All mutant values were normalized to WT.

Supplemental Fig. S27. The *dim-3* strain shows a decrease in strong intra-chromosomal contacts but an increase in strong inter-chromosomal contacts.

[A-B] Circos plot of the strongest intra-chromosomal contacts within LGII [A], or LGVII [B] at 10 kb resolution after normalizing for genomic distance. Black links indicate contacts with a $\log_2$ enrichment ≥2.25. Contact frequencies are indicated by differences in line thickness.

Supplemental Fig. S28. Number and distribution of telomeric foci in WT and *dim-3* nuclei.

[A] Bar graph displaying the percent of nuclei with 1-7 foci in WT (dark gray; n = 324 nuclei) or *dim-3* (light gray; n = 366 nuclei) strains. No significant changes were found ($p<0.01$; X^2 test). [B] Bar graph displaying the percent of all telomeric (TRF-1-GFP) foci that fall in Zones 1-3 in WT (dark gray; n = 1025 foci) or *dim-3* (light gray; n = 1105 foci) strains. Asterisks denote significant changes ($p<0.01$; Zone 1 p-value = 1.6×10^{-5}; Zone 2 p-value = 0.008; Zone 3 p-value = 1.0×10^{-13}; X^2 test); p-value = 2.5×10^{-18} (X^2 test) of all Zone differences between WT and
dim-3.

Supplemental Fig. S29. *In silico* chromosome modeling of WT genome reveals a "clothespin" chromosome configuration.

[A] Three-dimensional models of all *N. crassa* chromosomes (LGI - LGVII) shown as wire

diagrams. The paths of the wires pass through the center of a series of 50 kb "spheres". The relative conformations of the spheres were determined using the contact frequencies in the WT Hi-C dataset to set attractive or repulsive forces between each sphere and allowing the system to relax to a low energy state. Red color indicates regions enriched with the heterochromatic mark H3K9me3. The centromere and subtelomeres (labeled with arrows) appear separate from one another while the euchromatin emanates from the bundled heterochromatin.

Supplemental Fig. S30. *In silico* chromosome modeling of mutant genomes.
Three-dimensional models of *N. crassa* LGII (left) and LGVII (right) shown as continuous wire diagrams (see Supplemental Fig. S29) of [A] WT, [B] Δ*dim-5*, [C] Δ*hpo*, and [D] *dim-3* strains. Increasing red color indicates regions enriched with the heterochromatic mark H3K9me3. Centromeric and subtelomeric regions are labeled with arrows.

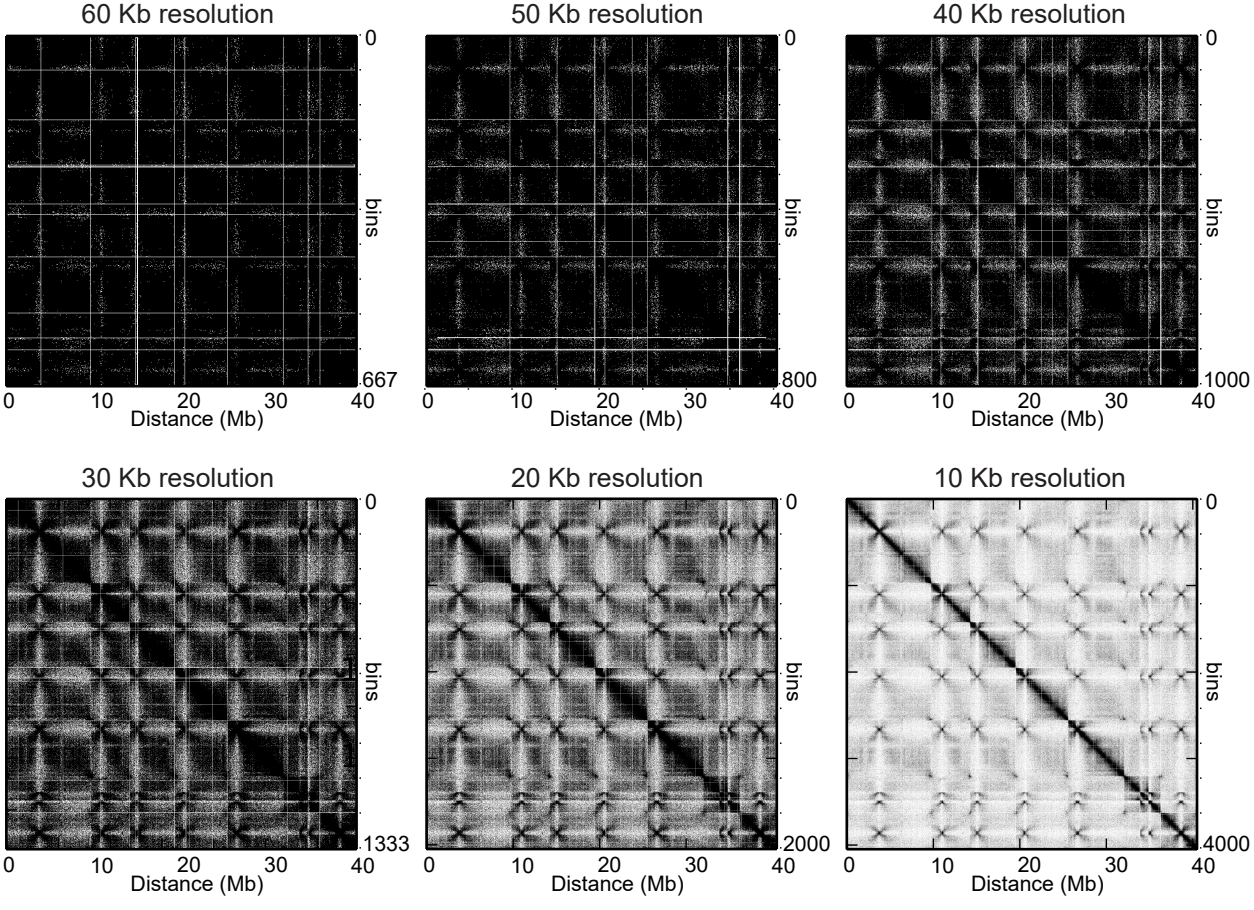
60 Kb resolution
50 Kb resolution
40 Kb resolution
30 Kb resolution
20 Kb resolution
10 Kb resolution
bins
0
667
800
1000
1333
2000
4000
0
10
20
30
40
Distance (Mb)

A

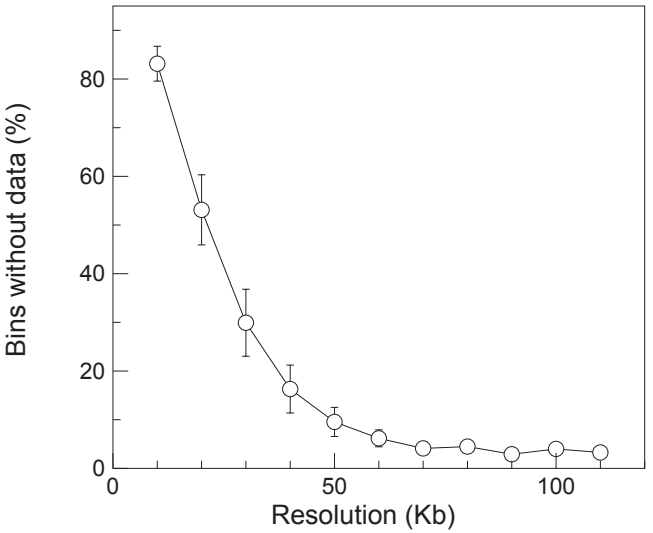
Bins without data (%)
0
20
40
60
80
0
50
100
Resolution (Kb)

B

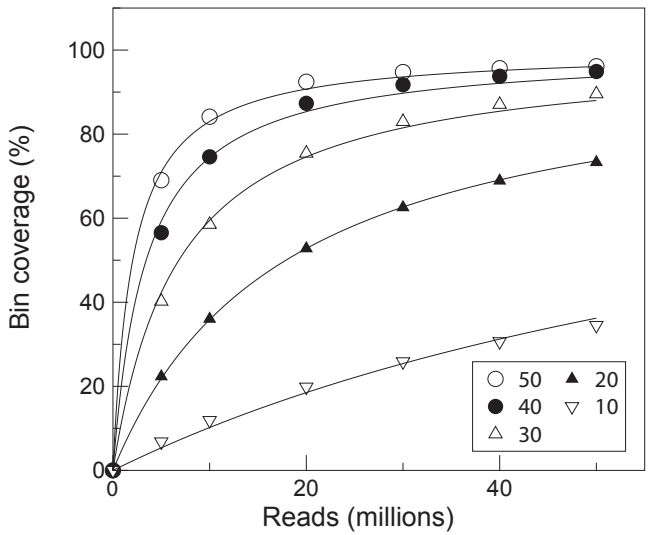
Bin coverage (%)
0
20
40
60
80
100
0
20
40
Reads (millions)
50
40
30
20
10

A

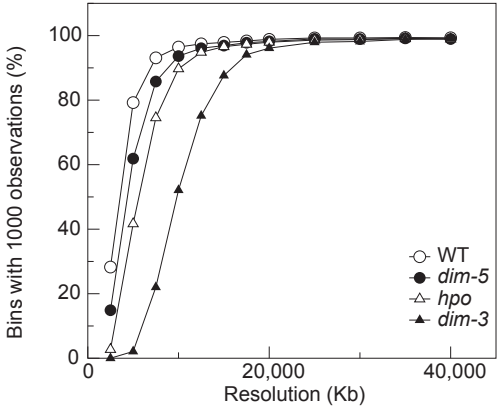

B

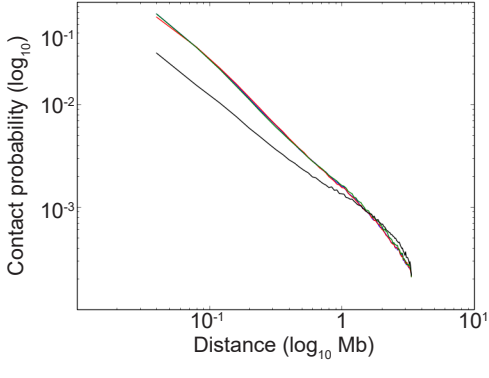

WT slope = -1.1575, r^2= 0.9976

Δ*dim-5* slope = -1.1664, r^2= 0.9985

Δ*hpo* slope = -1.1149, r^2= 0.9971

***dim-3* slope = -0.8295, r^2= 0.9965**

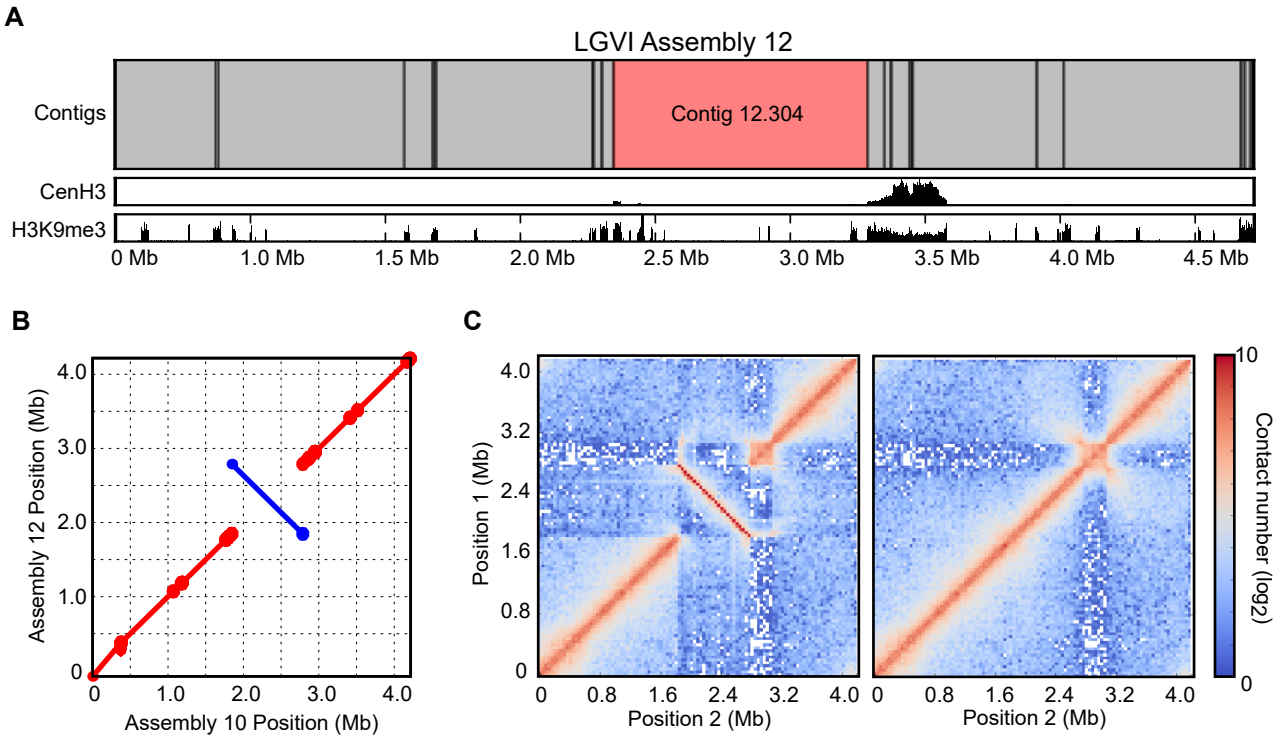
A
LGVI Assembly 12
Contigs
Contig 12.304
CenH3
H3K9me3
0 Mb
1.0 Mb
1.5 Mb
2.0 Mb
2.5 Mb
3.0 Mb
3.5 Mb
4.0 Mb
4.5 Mb
B
Assembly 12 Position (Mb)
Assembly 10 Position (Mb)
C
Position 1 (Mb)
Position 2 (Mb)
Position 2 (Mb)
Contact number (log2)

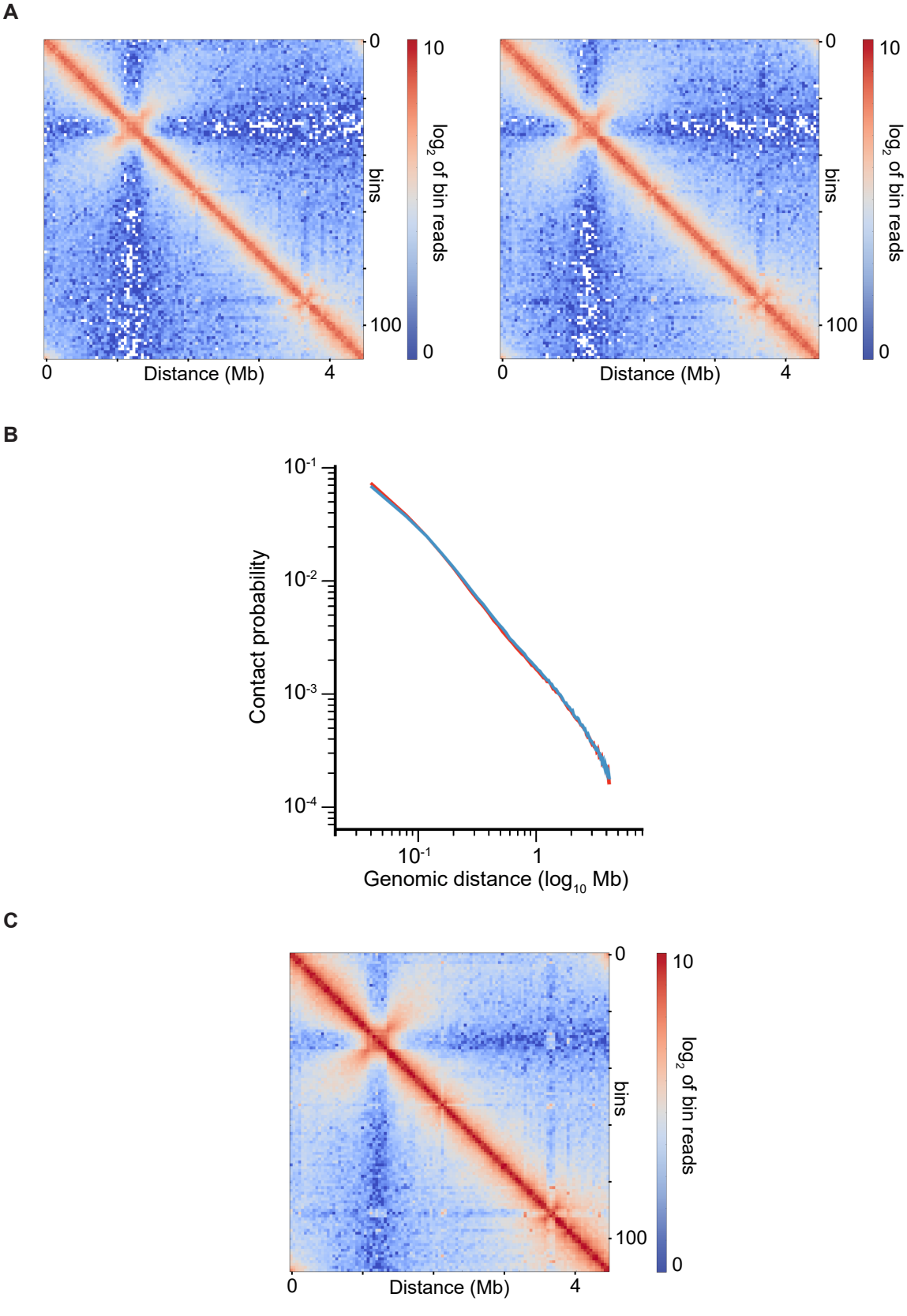
A
0
bins
100
0
Distance (Mb)
4
10
0
log2 of bin reads
B
Contact probability
10-1
10-2
10-3
10-4
10-1
1
Genomic distance (log10 Mb)
C

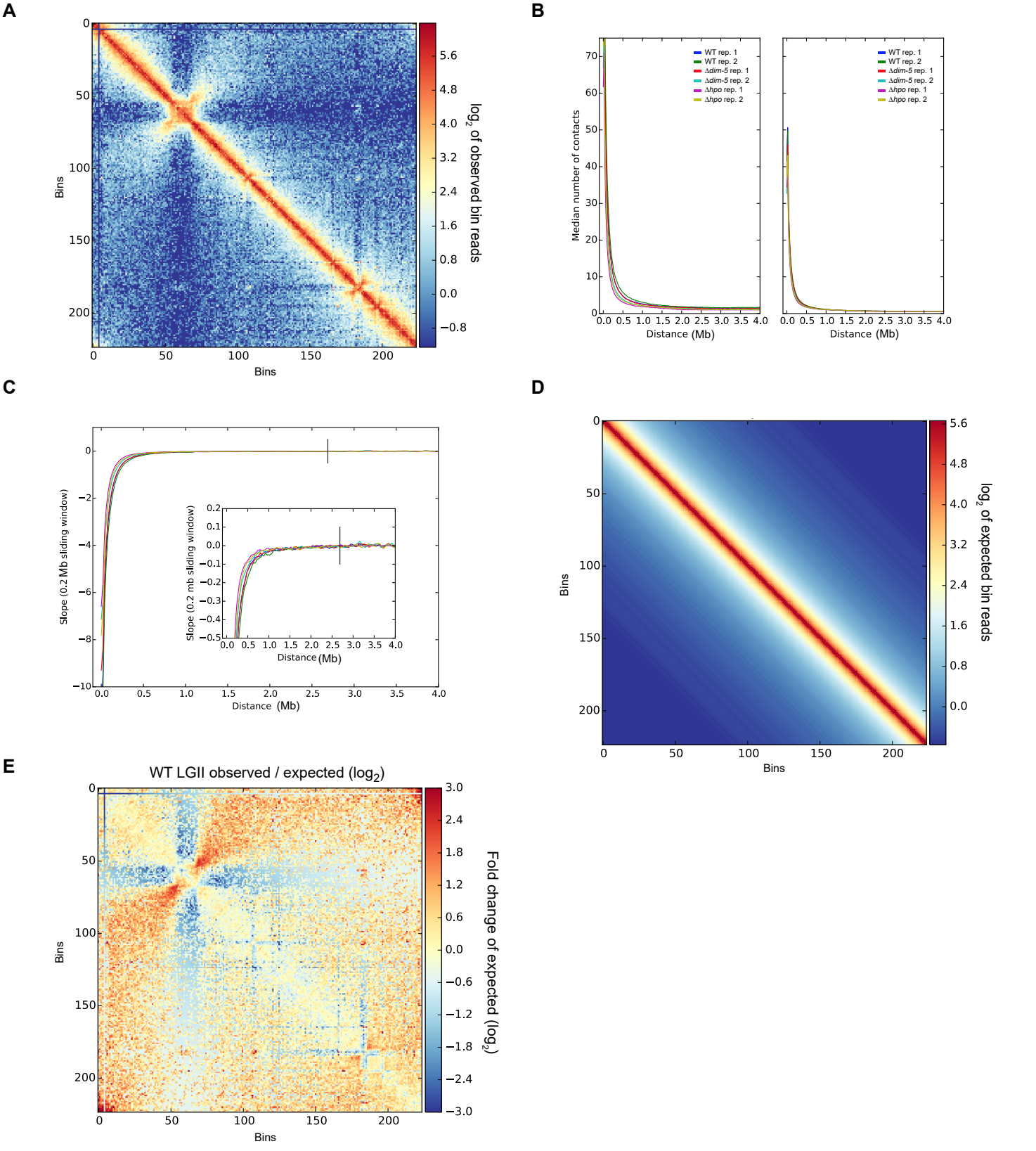
A
Bins
Bins
log2 of observed bin reads
B
Median number of contacts
Distance (Mb)
Distance (Mb)
WT rep. 1
WT rep. 2
Δdim-5 rep. 1
Δdim-5 rep. 2
Δhpo rep. 1
Δhpo rep. 2
C
Slope (0.2 Mb sliding window)
Distance (Mb)
Slope (0.2 mb sliding window)
Distance (Mb)
D
Bins
Bins
log2 of expected bin reads
E
WT LGII observed / expected (log2)
Bins
Bins
Fold change of expected (log2)

Supplemental Fig. 7

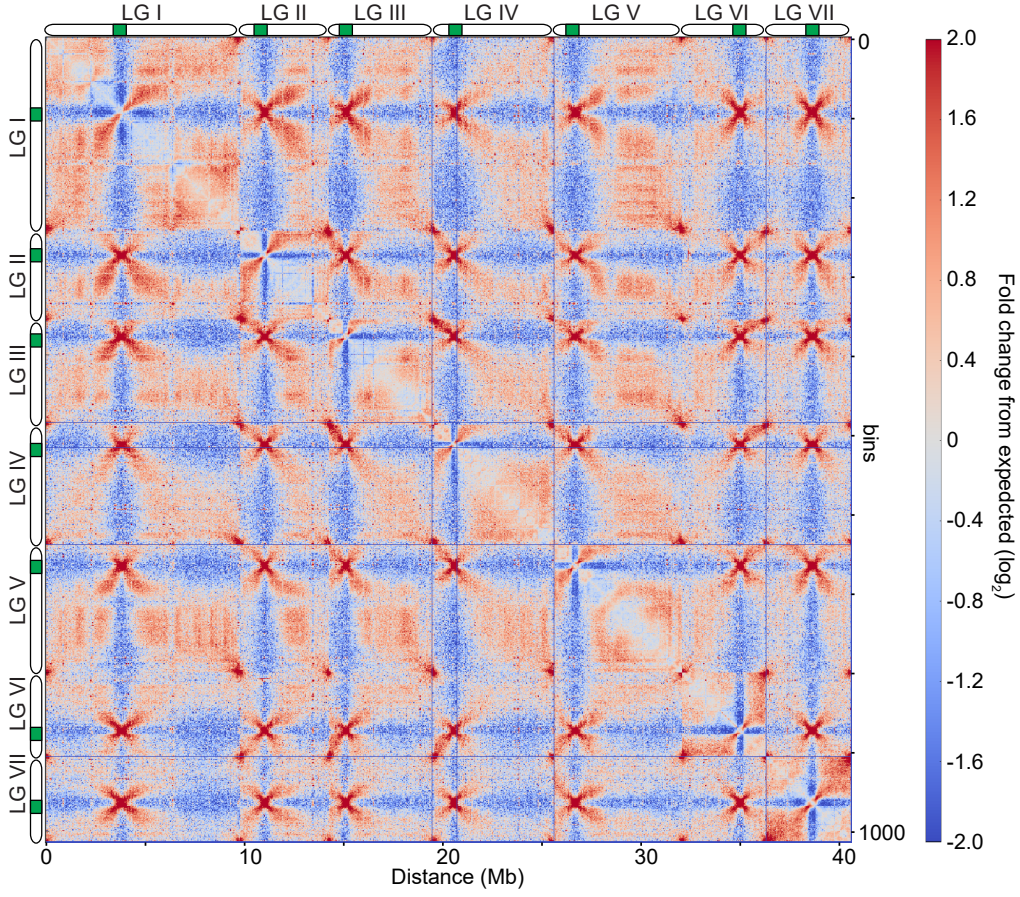

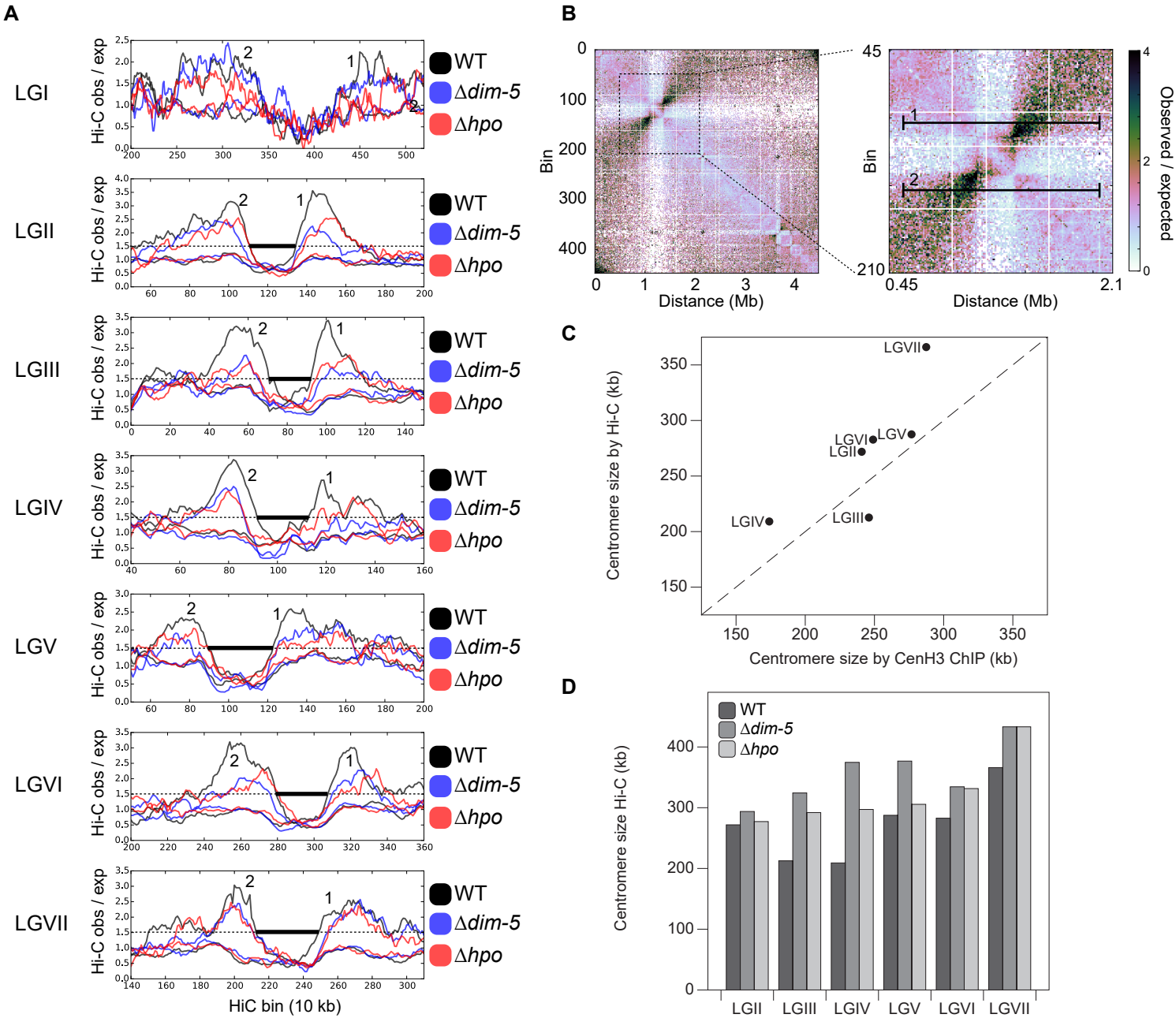
A
LGI
LGII
LGIII
LGIV
LGV
LGVI
LGVII
Hi-C obs / exp
WT
Δdim-5
Δhpo
HiC bin (10 kb)
B
Bin
Distance (Mb)
Observed / expected
C
Centromere size by Hi-C (kb)
Centromere size by CenH3 ChIP (kb)
LGVII
LGVI
LGV
LGII
LGIII
LGIV
D
Centromere size Hi-C (kb)
WT
Δdim-5
Δhpo
LGII
LGIII
LGIV
LGV
LGVI
LGVII

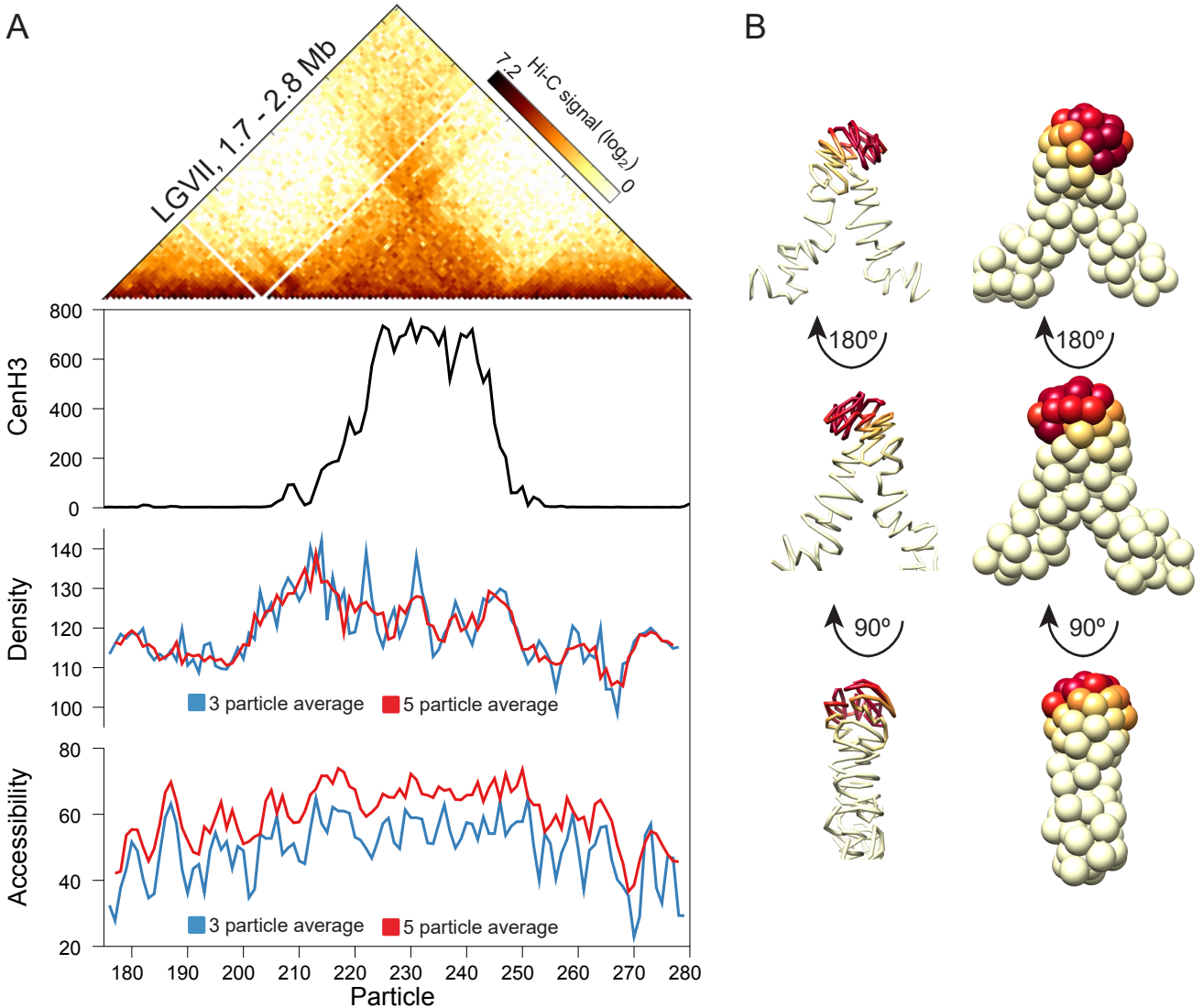
A
LGVII, 1.7 - 2.8 Mb
7.2
Hi-C signal (log2)
0
CenH3
800
600
400
200
0
Density
140
130
120
110
100
3 particle average
5 particle average
Accessibility
80
60
40
20
3 particle average
5 particle average
180
190
200
210
220
230
240
250
260
270
280
Particle
B
180°
180°
90°
90°

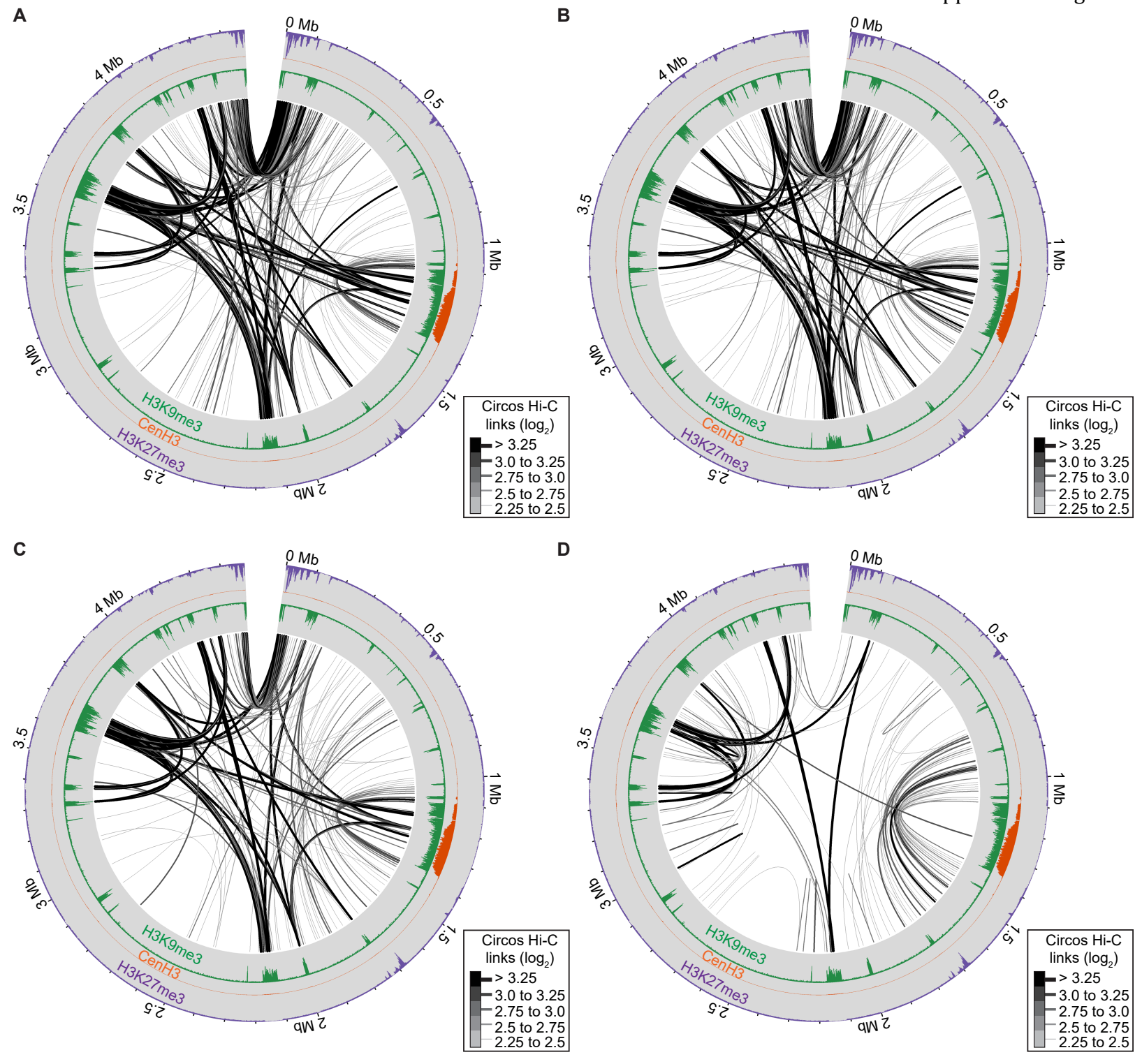
A
B
C
D
0 Mb
0.5
1 Mb
1.5
2 Mb
2.5
3 Mb
3.5
4 Mb
H3K9me3
CenH3
H3K27me3
Circos Hi-C links (log2)
> 3.25
3.0 to 3.25
2.75 to 3.0
2.5 to 2.75
2.25 to 2.5

Supplemental Fig. 11

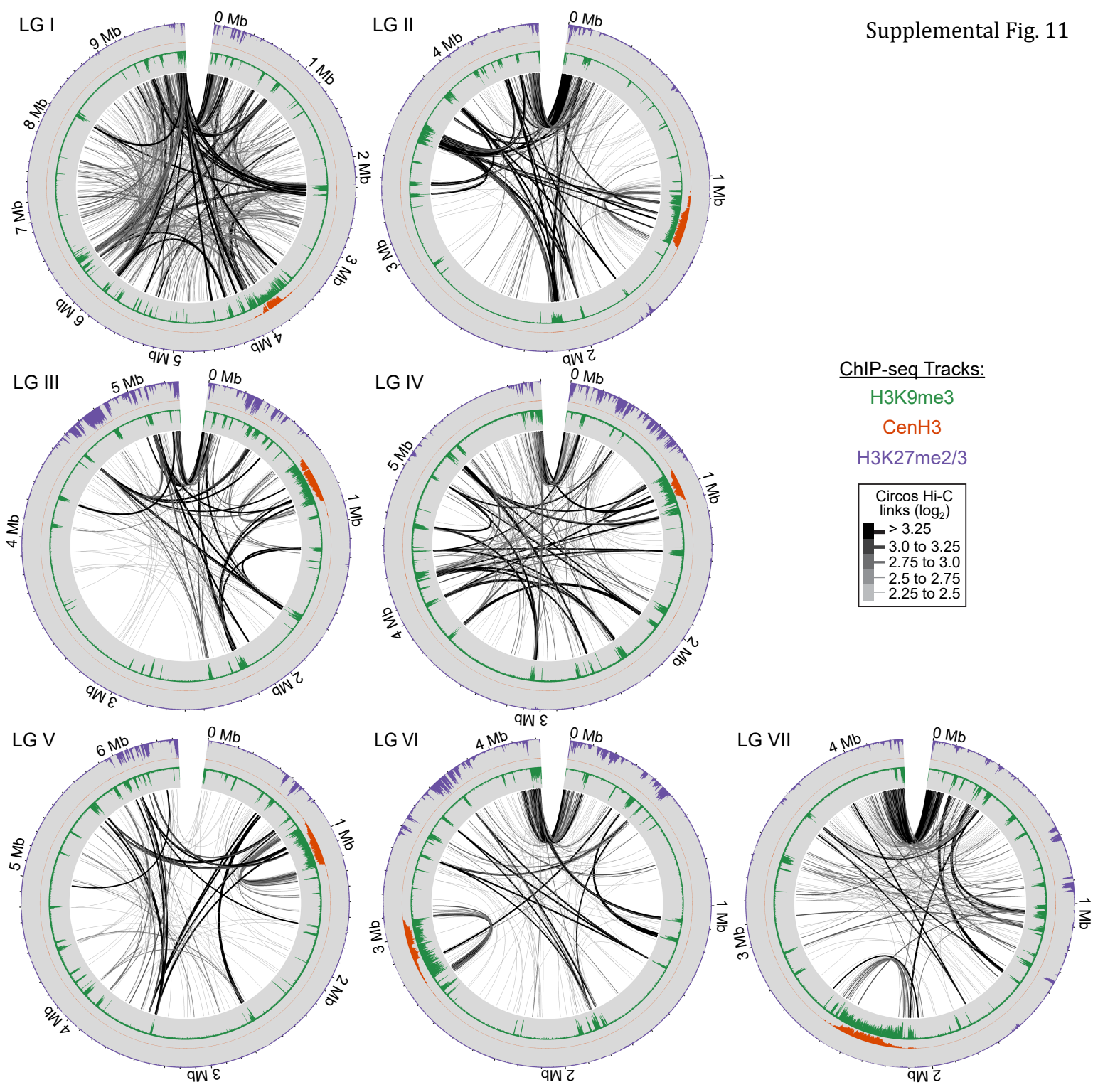

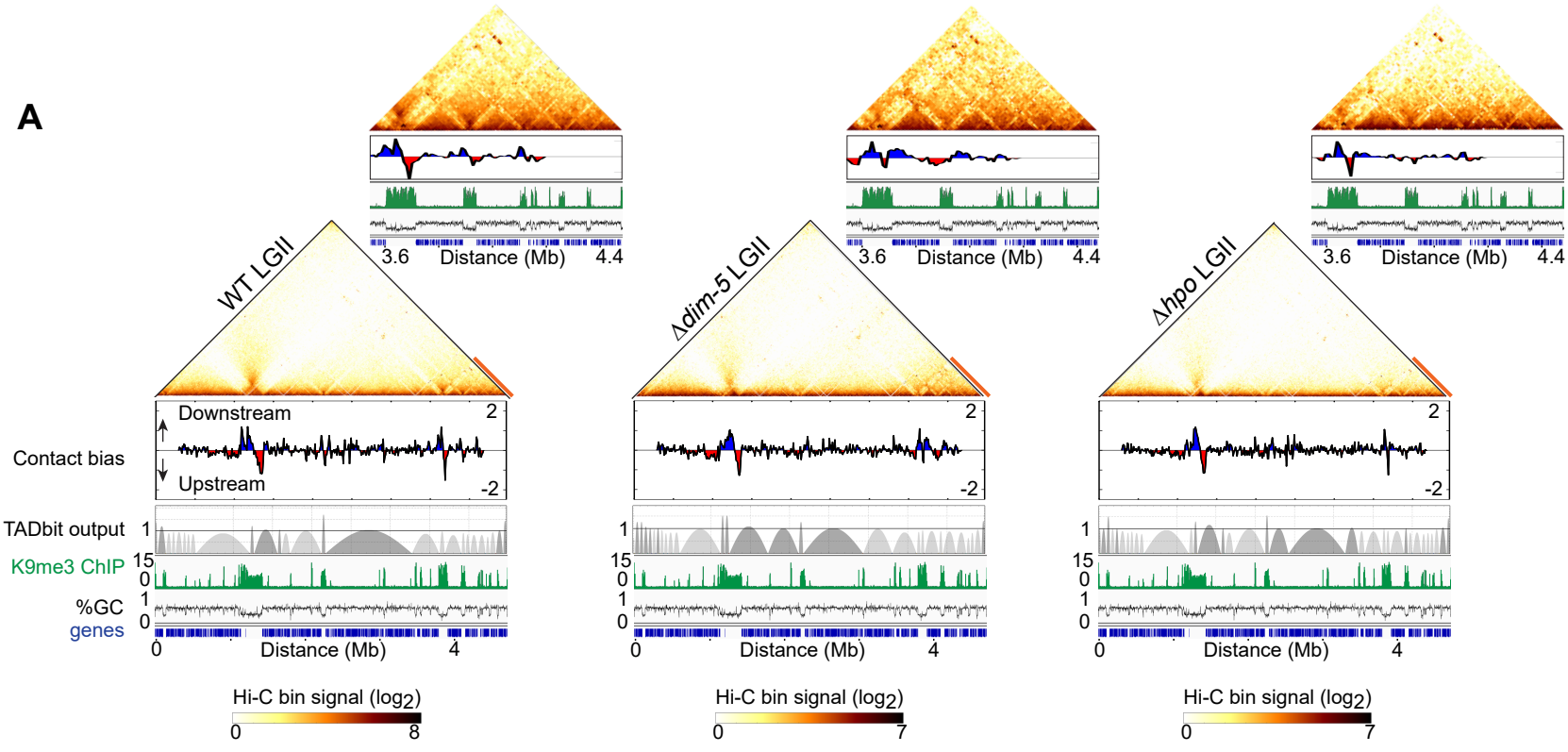
A
WT LGII
Δdim-5 LGII
Δhpo LGII
3.6
Distance (Mb)
4.4
Contact bias
Downstream
Upstream
2
-2
TADbit output
K9me3 ChIP
%GC
genes
0
4
Hi-C bin signal (log2)
0
8
7

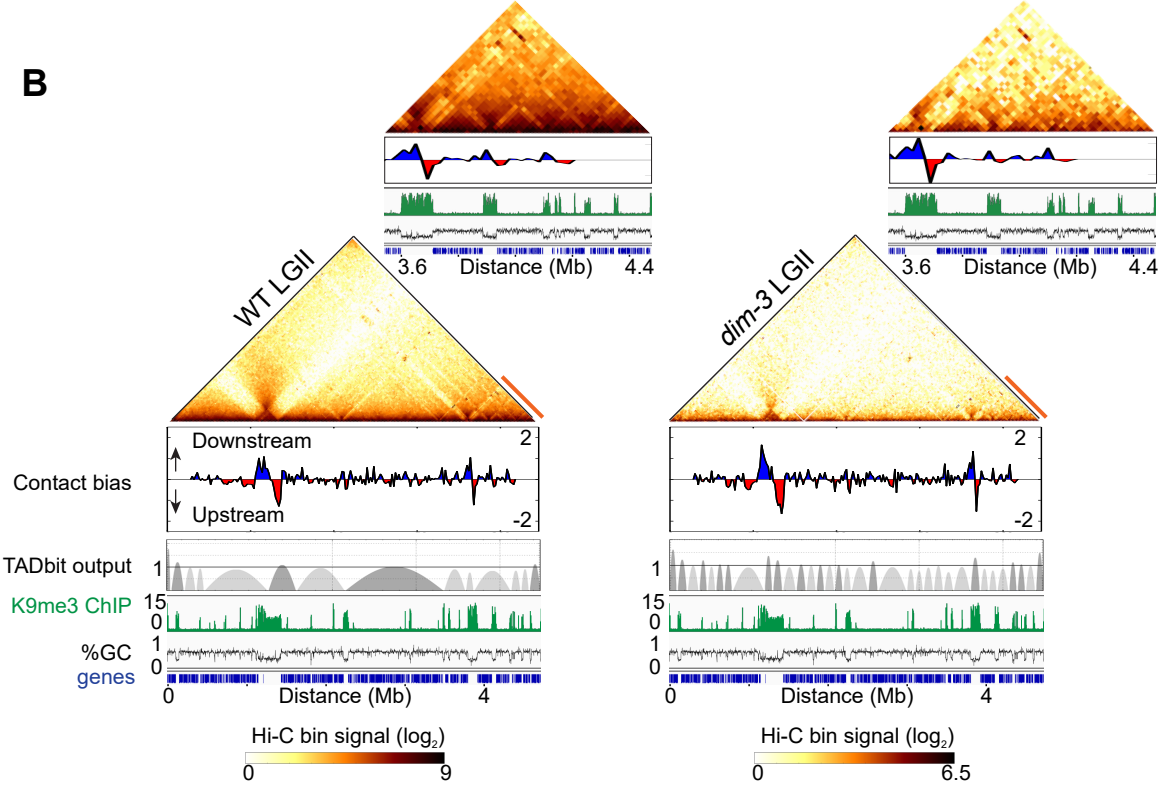
B
WT LGII
dim-3 LGII
3.6
Distance (Mb)
4.4
Contact bias
Downstream
Upstream
2
-2
TADbit output
K9me3 ChIP
%GC
genes
0
4
Hi-C bin signal (log2)
0
9
6.5

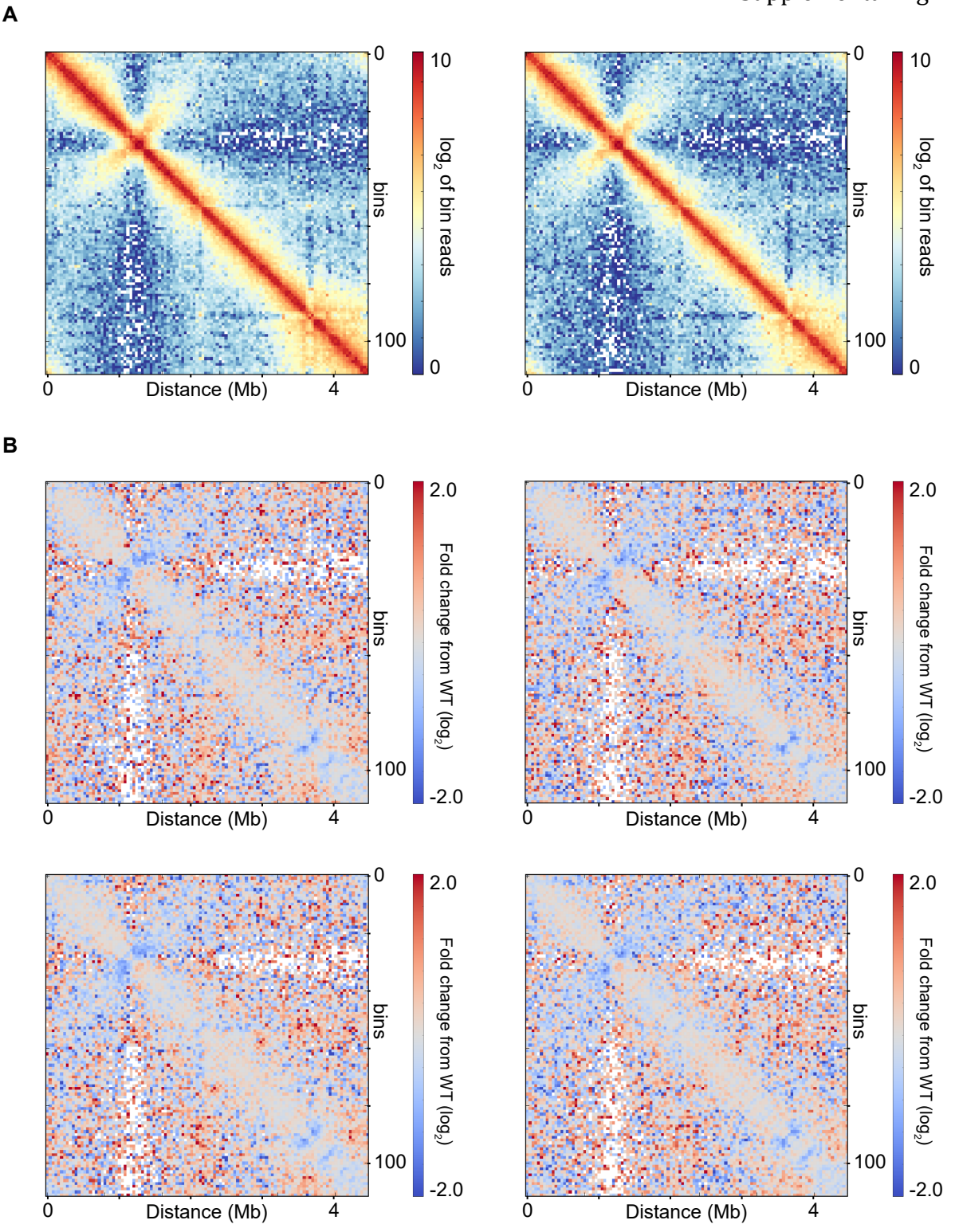
A
0
bins
100
0
Distance (Mb)
4
10
log2 of bin reads
0
B
2.0
Fold change from WT (log2)
-2.0

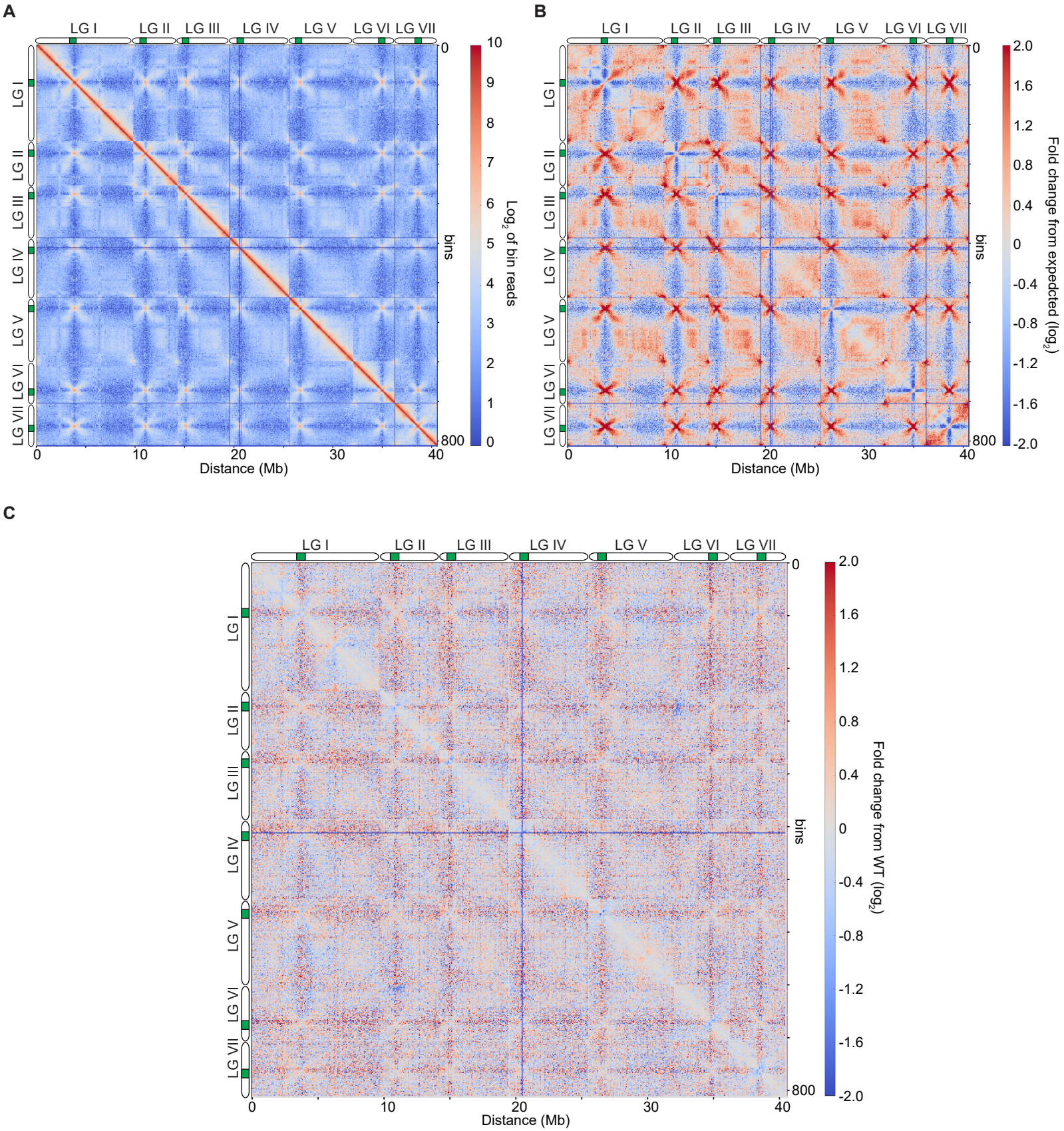
A
B
C
LG I
LG II
LG III
LG IV
LG V
LG VI
LG VII
bins
0
800
Distance (Mb)
0
10
20
30
40
Log2 of bin reads
Fold change from expected (log2)
Fold change from WT (log2)
10
9
8
7
6
5
4
3
2
1
2.0
1.6
1.2
0.8
0.4
-0.4
-0.8
-1.2
-1.6
-2.0

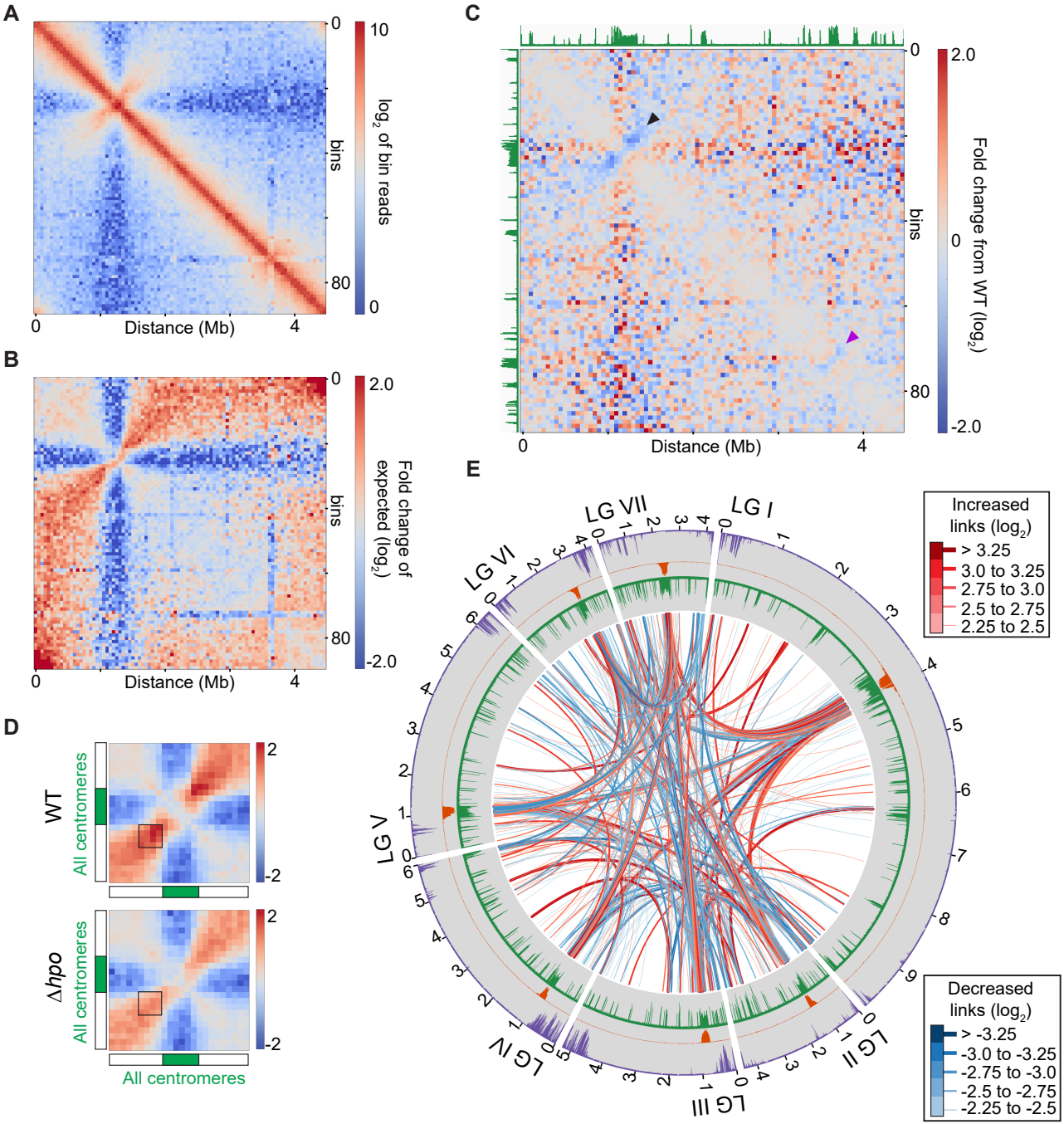
A
0
bins
80
0
Distance (Mb)
4
10
log2 of bin reads
0
B
0
bins
80
0
Distance (Mb)
4
2.0
Fold change of expected (log2)
-2.0
C
0
bins
80
0
Distance (Mb)
4
2.0
Fold change from WT (log2)
0
-2.0
D
WT
All centromeres
2
-2
Δhpo
All centromeres
2
-2
All centromeres
E
LG I
LG II
LG III
LG IV
LG V
LG VI
LG VII
Increased links (log2)
> 3.25
3.0 to 3.25
2.75 to 3.0
2.5 to 2.75
2.25 to 2.5
Decreased links (log2)
> -3.25
-3.0 to -3.25
-2.75 to -3.0
-2.5 to -2.75
-2.25 to -2.5

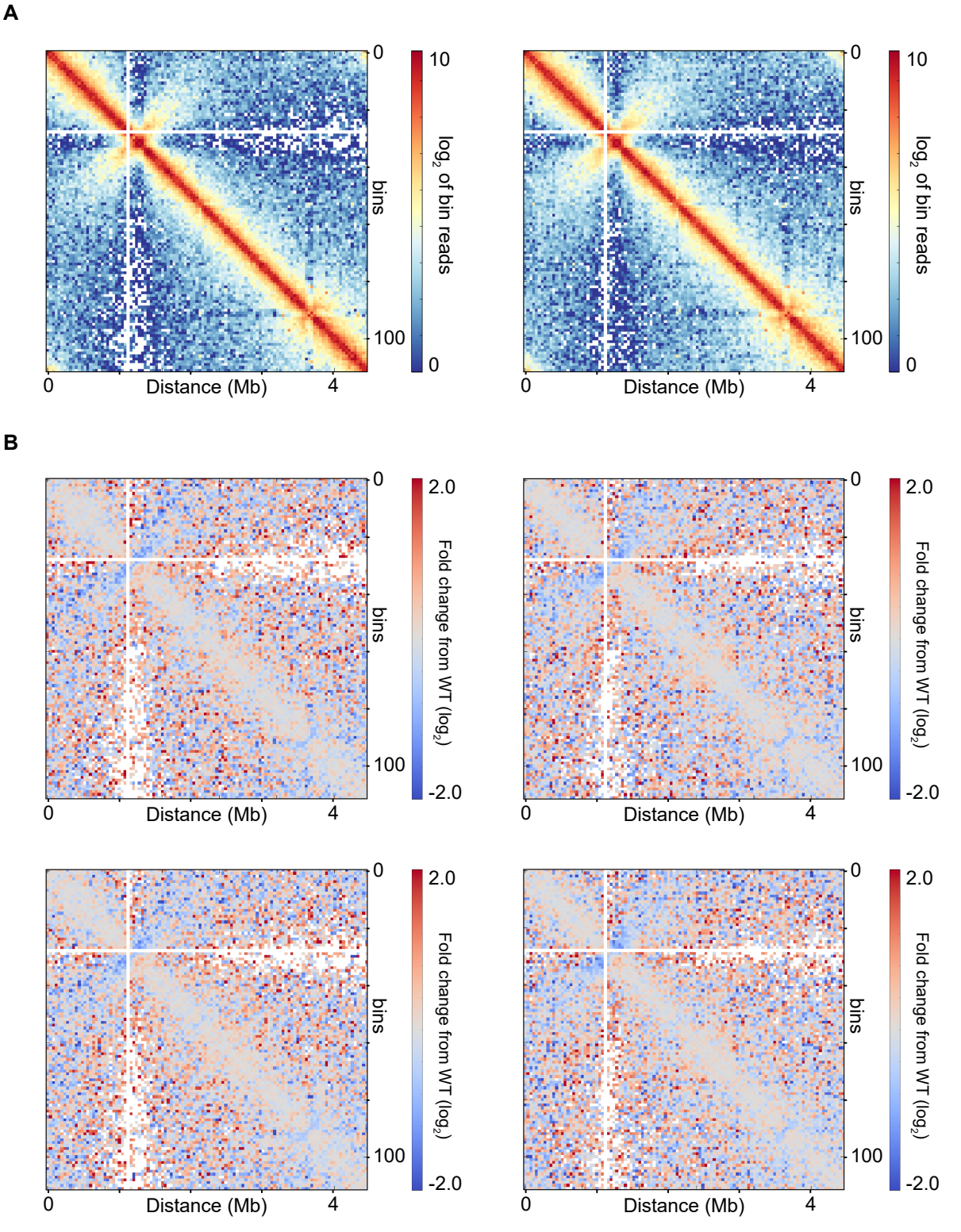
A
B
0
bins
100
Distance (Mb)
4
10
log2 of bin reads
2.0
Fold change from WT (log2)
-2.0

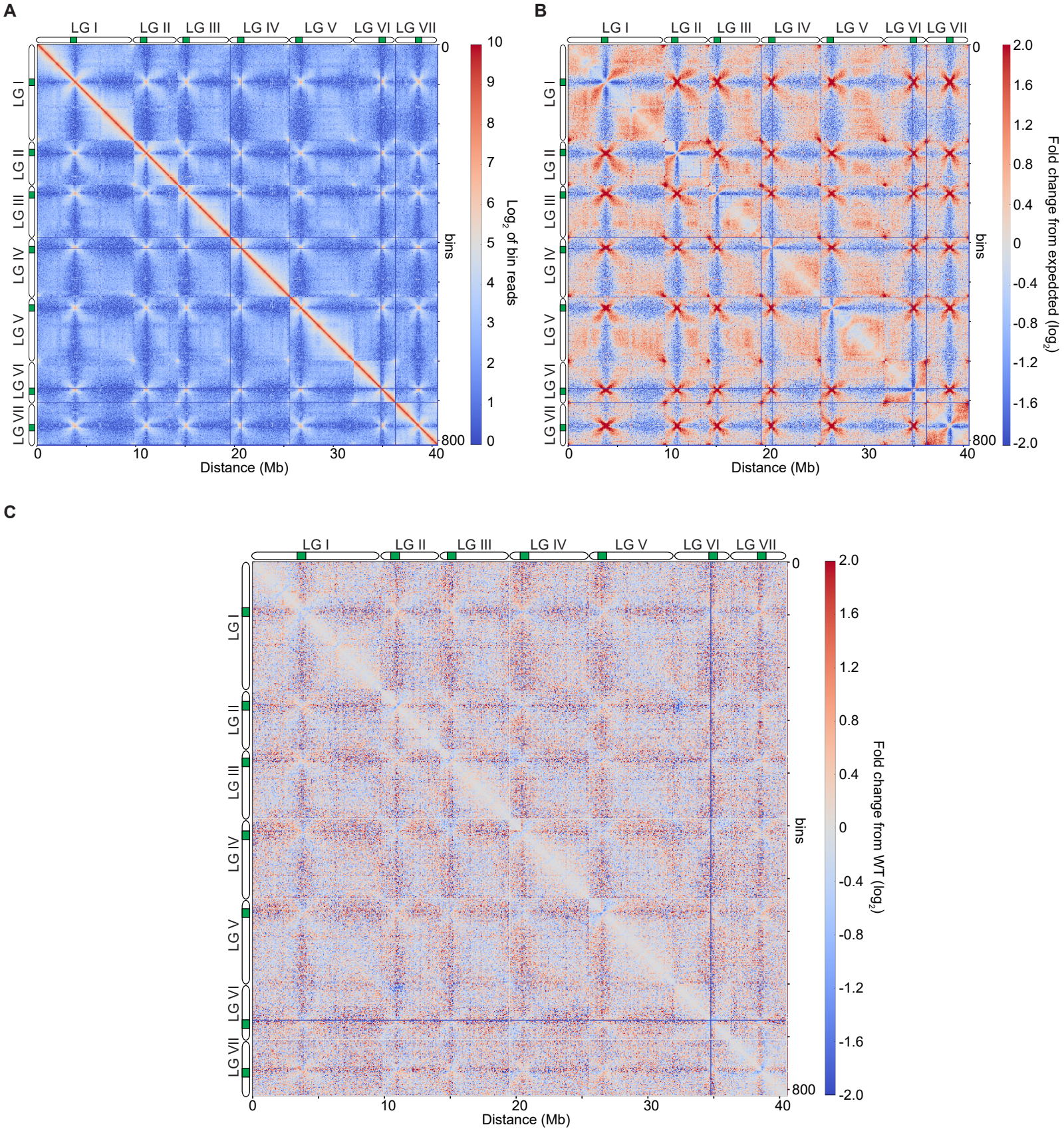
A
B
C
LG I
LG II
LG III
LG IV
LG V
LG VI
LG VII
bins
0
800
Distance (Mb)
0
10
20
30
40
Log2 of bin reads
0
1
2
3
4
5
6
7
8
9
10
Fold change from expected (log2)
Fold change from WT (log2)
-2.0
-1.6
-1.2
-0.8
-0.4
0
0.4
0.8
1.2
1.6
2.0

A

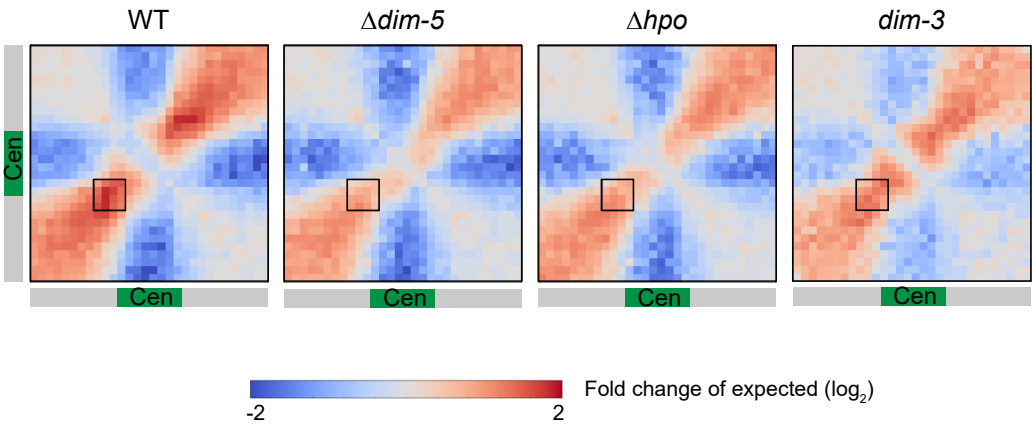
WT
Δdim-5
Δhpo
dim-3
Cen
Cen
Cen
Cen
Cen
Fold change of expected (log2)
-2
2

B

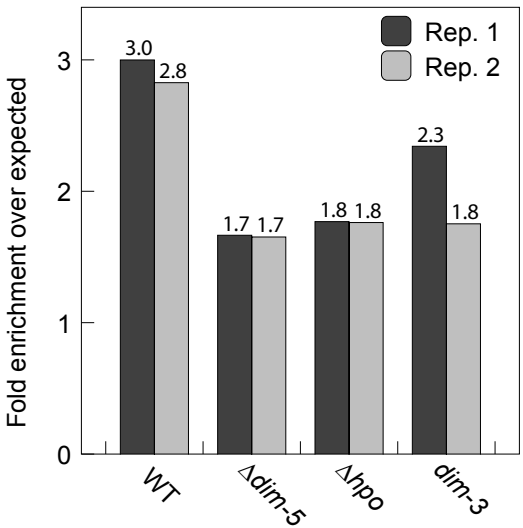
Rep. 1
Rep. 2
Fold enrichment over expected
0
1
2
3
3.0
2.8
1.7
1.7
1.8
1.8
2.3
1.8
WT
Δdim-5
Δhpo
dim-3

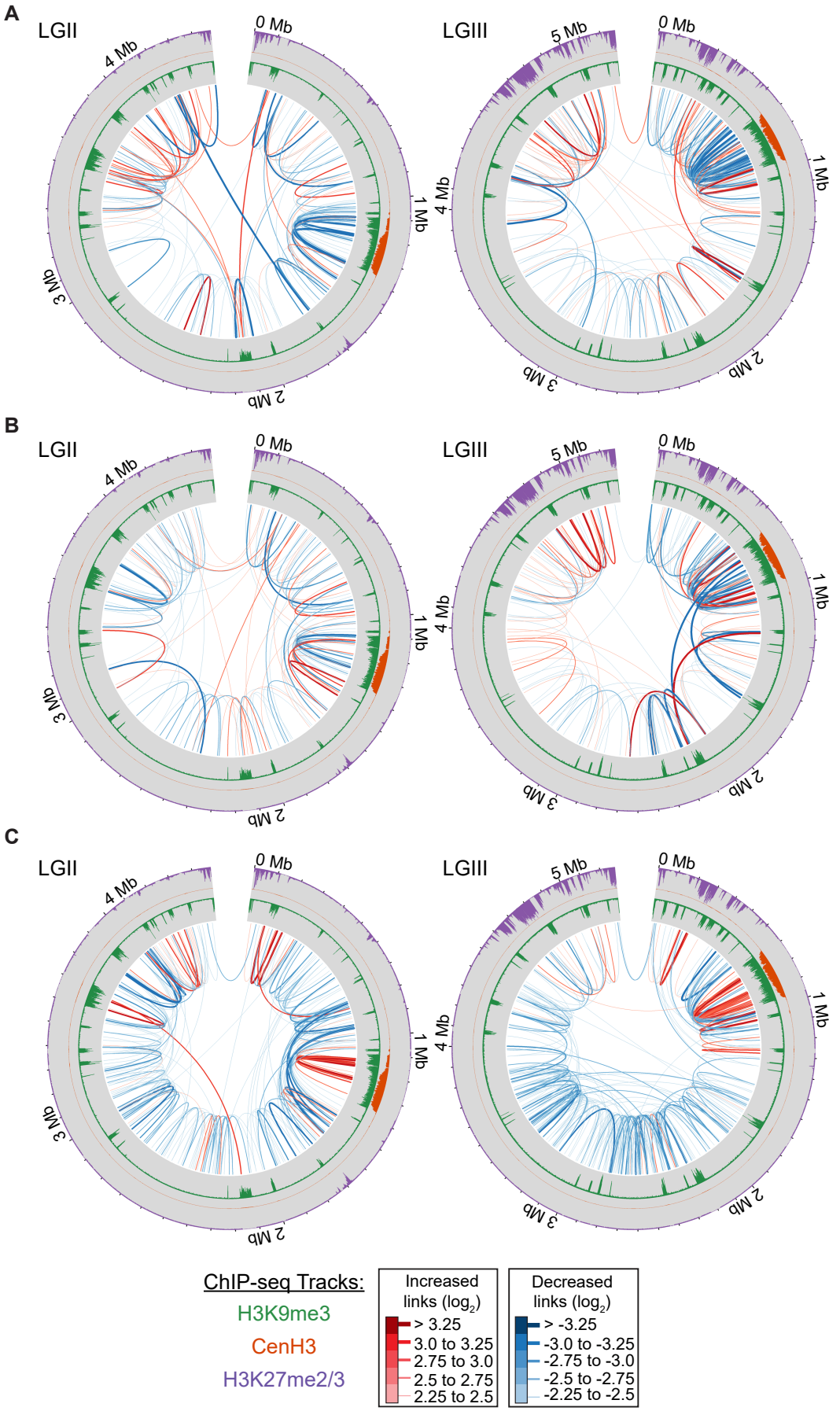
A
LGII
0 Mb
1 Mb
2 Mb
3 Mb
4 Mb
LGIII
0 Mb
1 Mb
2 Mb
3 Mb
4 Mb
5 Mb
B
LGII
0 Mb
1 Mb
2 Mb
3 Mb
4 Mb
LGIII
0 Mb
1 Mb
2 Mb
3 Mb
4 Mb
5 Mb
C
LGII
0 Mb
1 Mb
2 Mb
3 Mb
4 Mb
LGIII
0 Mb
1 Mb
2 Mb
3 Mb
4 Mb
5 Mb
ChIP-seq Tracks:
H3K9me3
CenH3
H3K27me2/3
Increased links (log2)
> 3.25
3.0 to 3.25
2.75 to 3.0
2.5 to 2.75
2.25 to 2.5
Decreased links (log2)
> -3.25
-3.0 to -3.25
-2.75 to -3.0
-2.5 to -2.75
-2.25 to -2.5

A

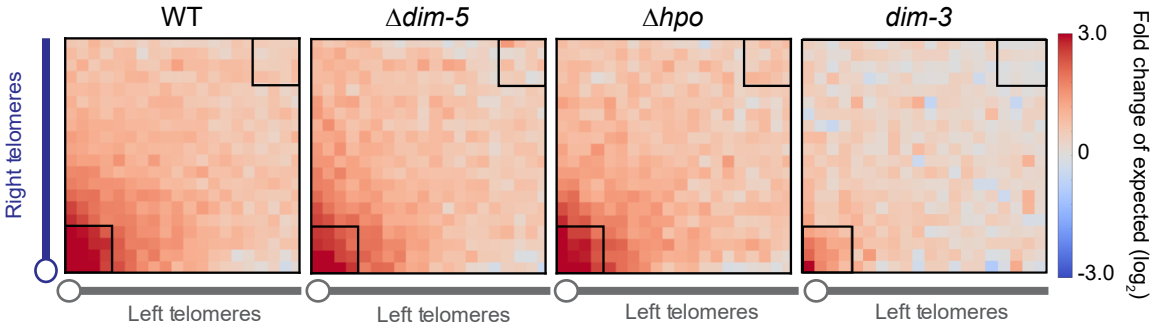
WT
Δdim-5
Δhpo
dim-3
Right telomeres
Left telomeres
Left telomeres
Left telomeres
Left telomeres
3.0
0
-3.0
Fold change of expected (log2)

B

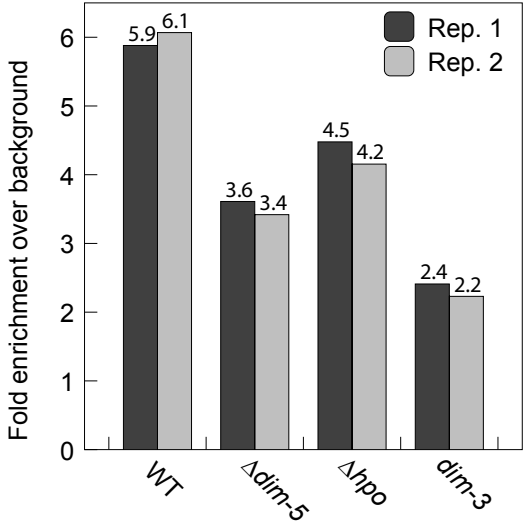
Fold enrichment over background
Rep. 1
Rep. 2
5.9
6.1
3.6
3.4
4.5
4.2
2.4
2.2
0
1
2
3
4
5
6
WT
Δdim-5
Δhpo
dim-3

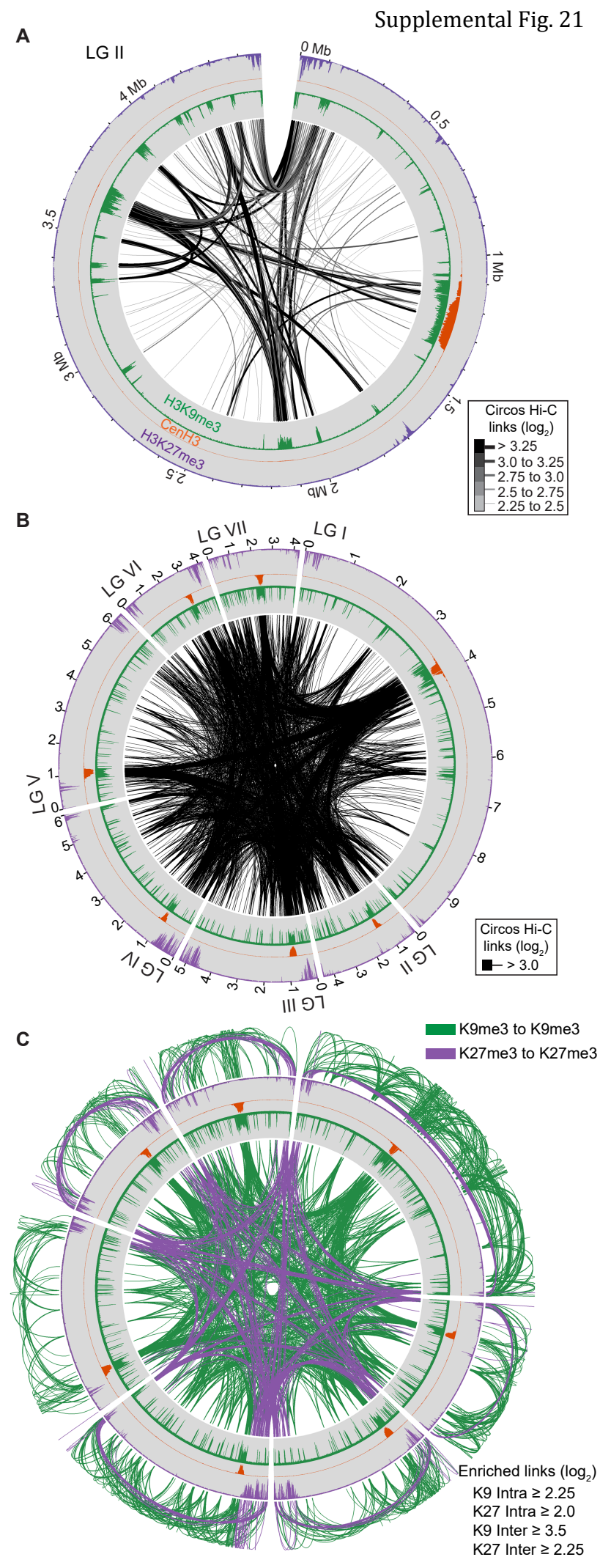
A
LG II
0 Mb
0.5
1 Mb
1.5
2 Mb
2.5
3 Mb
3.5
4 Mb
H3K9me3
CenH3
H3K27me3
Circos Hi-C links (log2)
> 3.25
3.0 to 3.25
2.75 to 3.0
2.5 to 2.75
2.25 to 2.5
B
LG I
LG II
LG III
LG IV
LG V
LG VI
LG VII
Circos Hi-C links (log2)
> 3.0
C
K9me3 to K9me3
K27me3 to K27me3
Enriched links (log2)
K9 Intra ≥ 2.25
K27 Intra ≥ 2.0
K9 Inter ≥ 3.5
K27 Inter ≥ 2.25

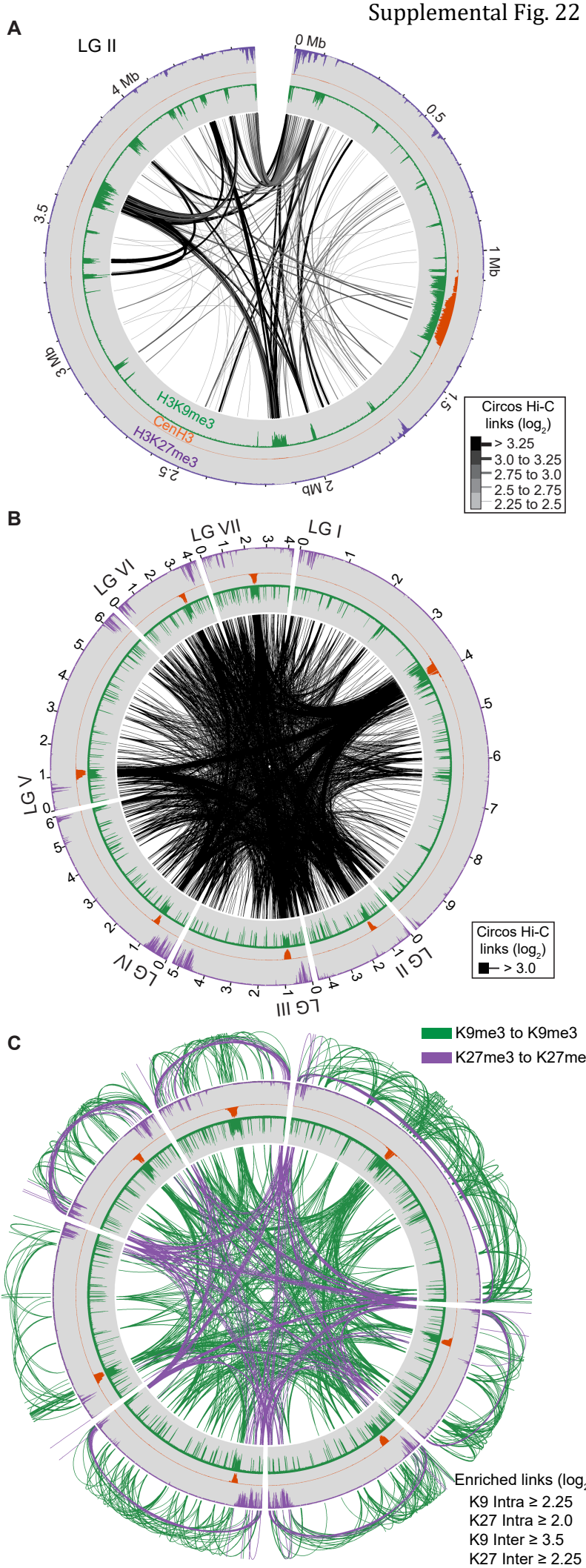
A
LG II
0 Mb
0.5
1 Mb
1.5
2 Mb
2.5
3 Mb
3.5
4 Mb
H3K9me3
CenH3
H3K27me3
Circos Hi-C links (log2)
> 3.25
3.0 to 3.25
2.75 to 3.0
2.5 to 2.75
2.25 to 2.5
B
LG I
LG II
LG III
LG IV
LG V
LG VI
LG VII
Circos Hi-C links (log2)
> 3.0
C
K9me3 to K9me3
K27me3 to K27me3
Enriched links (log2)
K9 Intra ≥ 2.25
K27 Intra ≥ 2.0
K9 Inter ≥ 3.5
K27 Inter ≥ 2.25

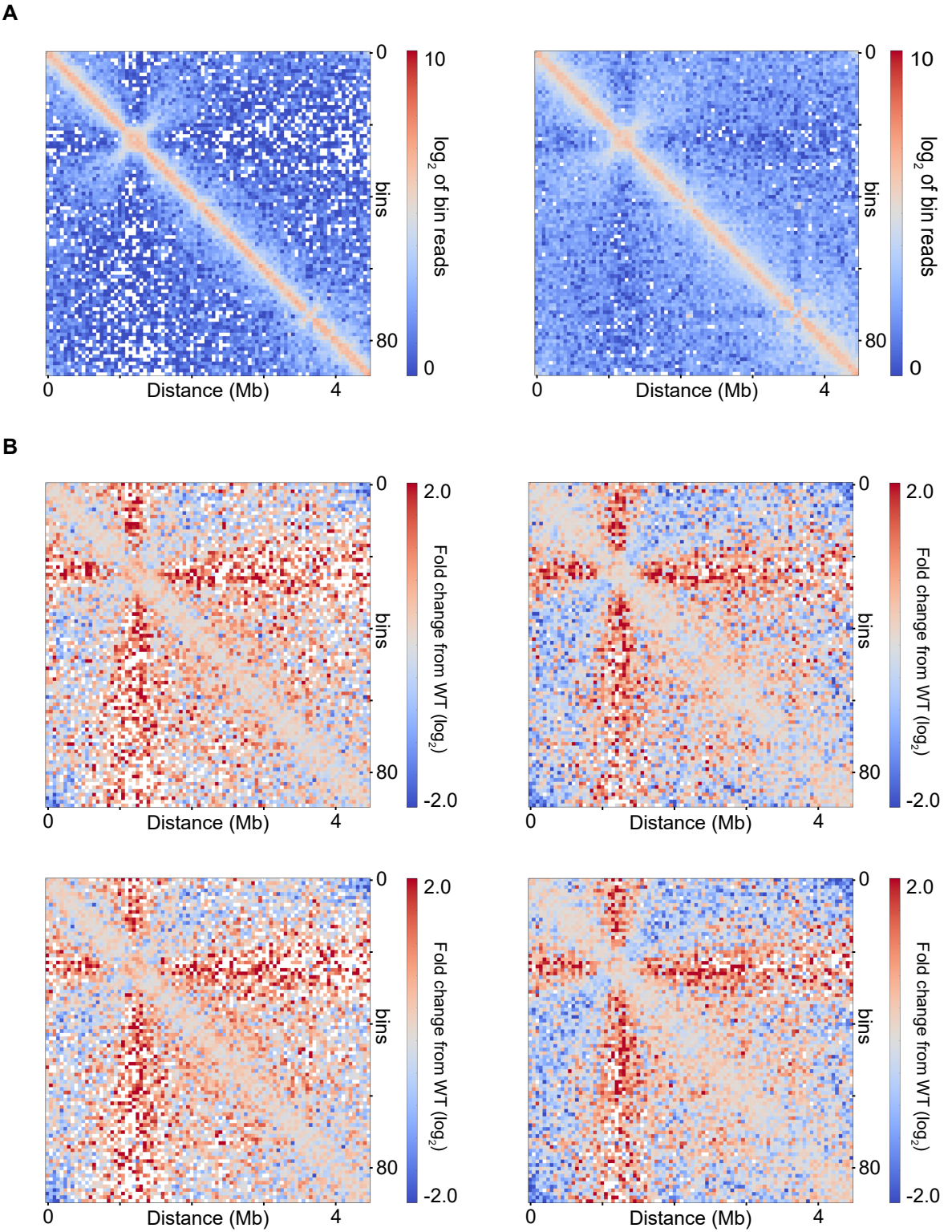
A
0
bins
80
0
Distance (Mb)
4
10
log2 of bin reads
0
B
2.0
Fold change from WT (log2)
-2.0

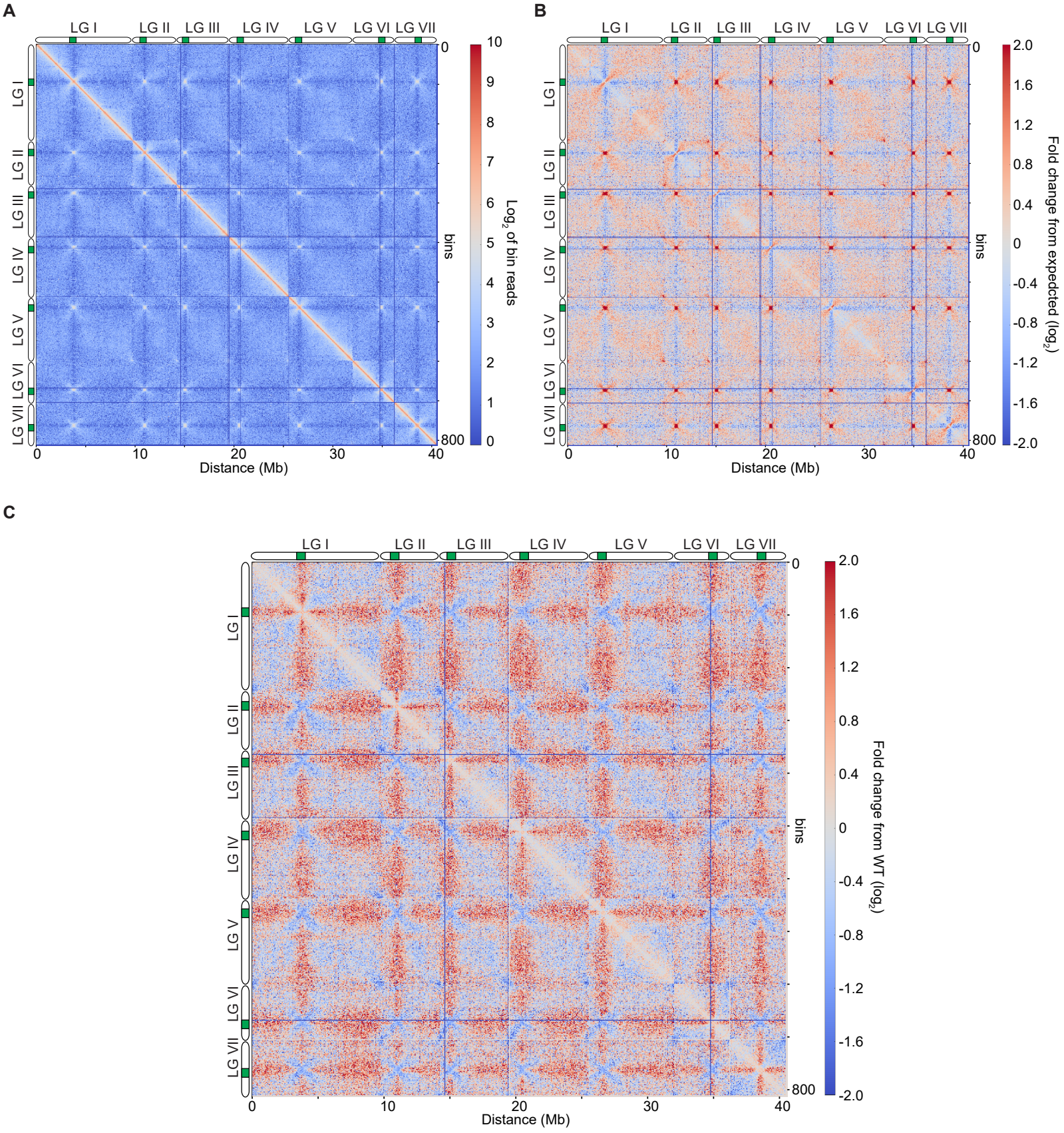
A
B
C
LG I
LG II
LG III
LG IV
LG V
LG VI
LG VII
bins
0
800
Distance (Mb)
0
10
20
30
40
Log2 of bin reads
Fold change from expected (log2)
Fold change from WT (log2)
2.0
1.6
1.2
0.8
0.4
0
-0.4
-0.8
-1.2
-1.6
-2.0

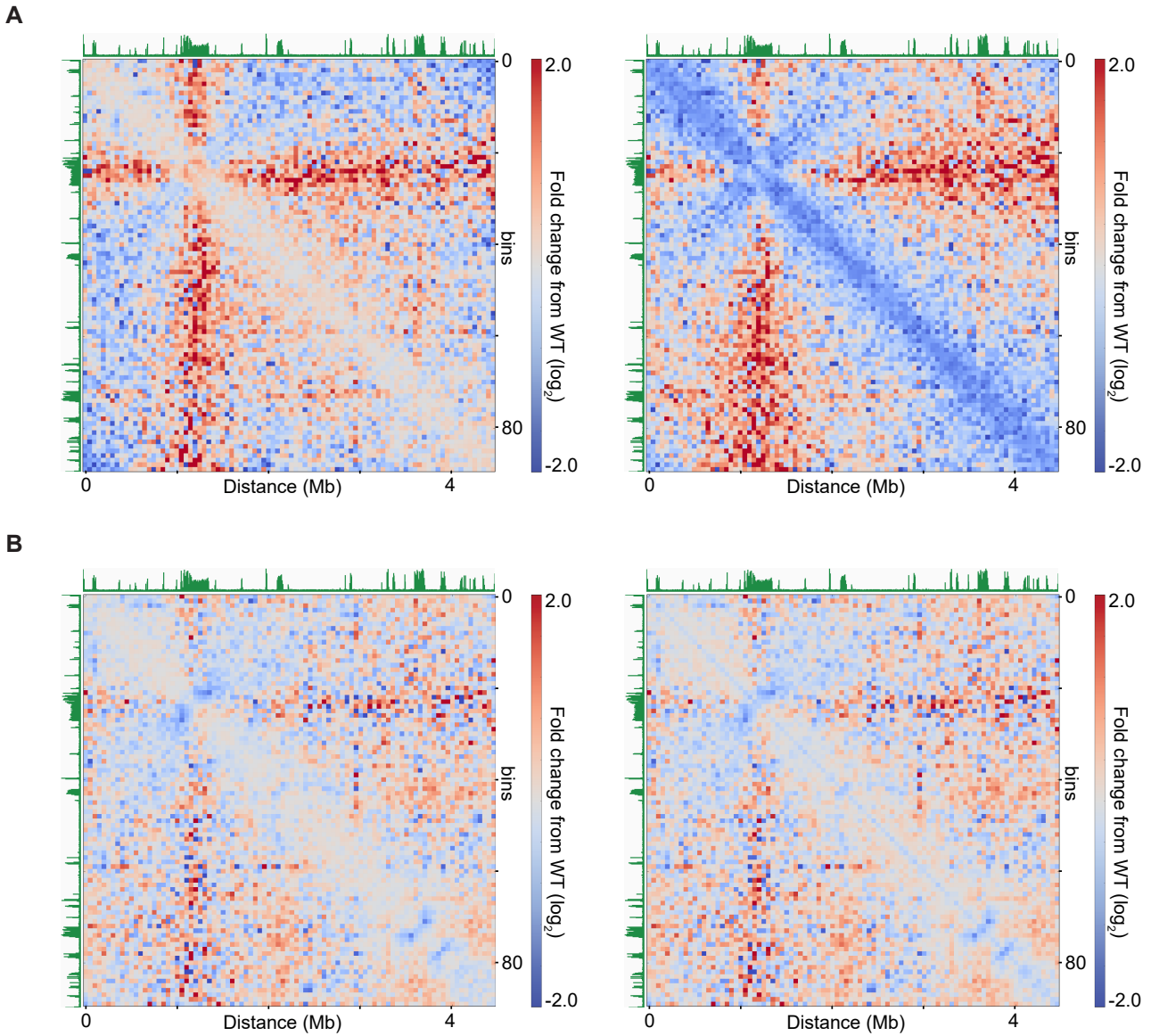
A
B
0
bins
80
0
Distance (Mb)
4
2.0
Fold change from WT (log2)
-2.0

Supplemental Fig. 26

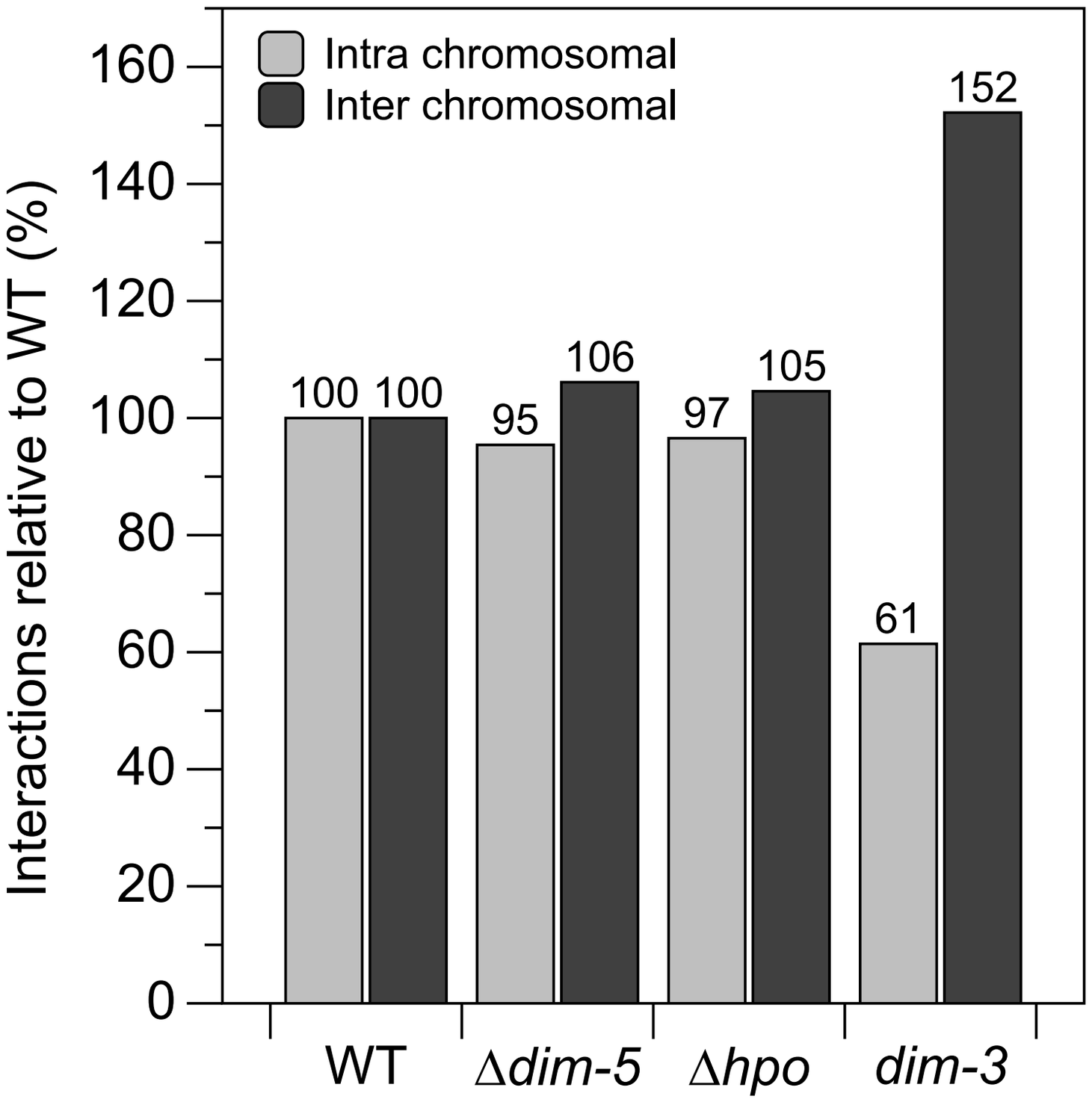

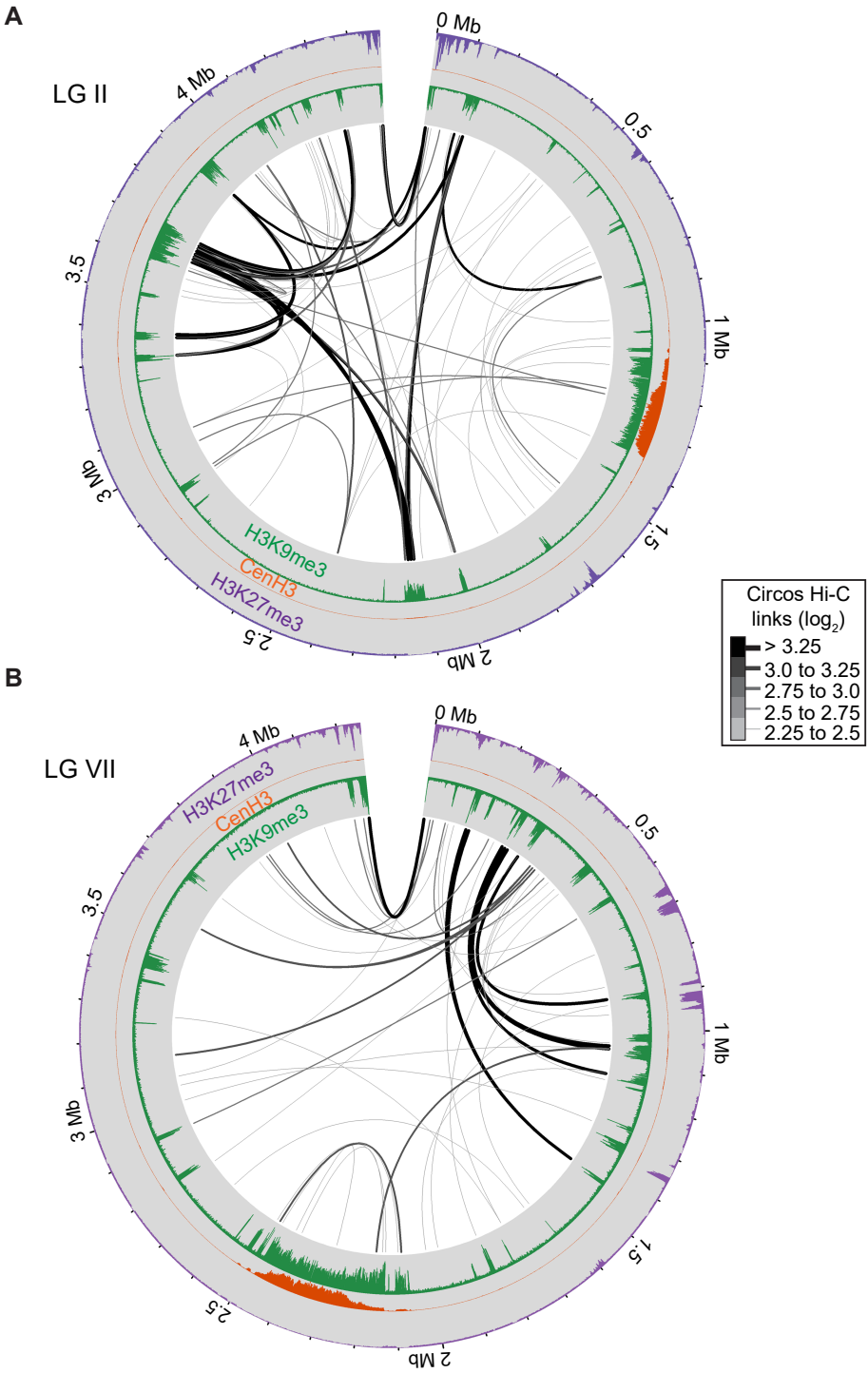
A
LG II
0 Mb
0.5
1 Mb
1.5
2 Mb
2.5
3 Mb
3.5
4 Mb
H3K9me3
CenH3
H3K27me3
Circos Hi-C links (log2)
> 3.25
3.0 to 3.25
2.75 to 3.0
2.5 to 2.75
2.25 to 2.5
B
LG VII
0 Mb
0.5
1 Mb
1.5
2 Mb
2.5
3 Mb
3.5
4 Mb
H3K27me3
CenH3
H3K9me3

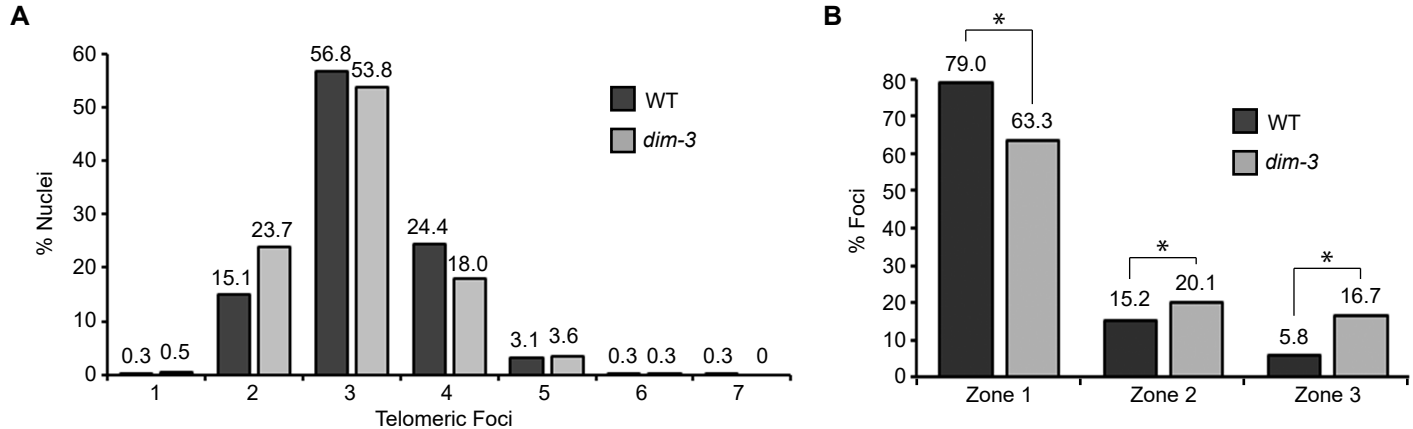
A
% Nuclei
Telomeric Foci
WT
dim-3
0.3
0.5
15.1
23.7
56.8
53.8
24.4
18.0
3.1
3.6
0.3
0.3
0.3
0
1
2
3
4
5
6
7
B
% Foci
79.0
63.3
15.2
20.1
5.8
16.7
*
Zone 1
Zone 2
Zone 3

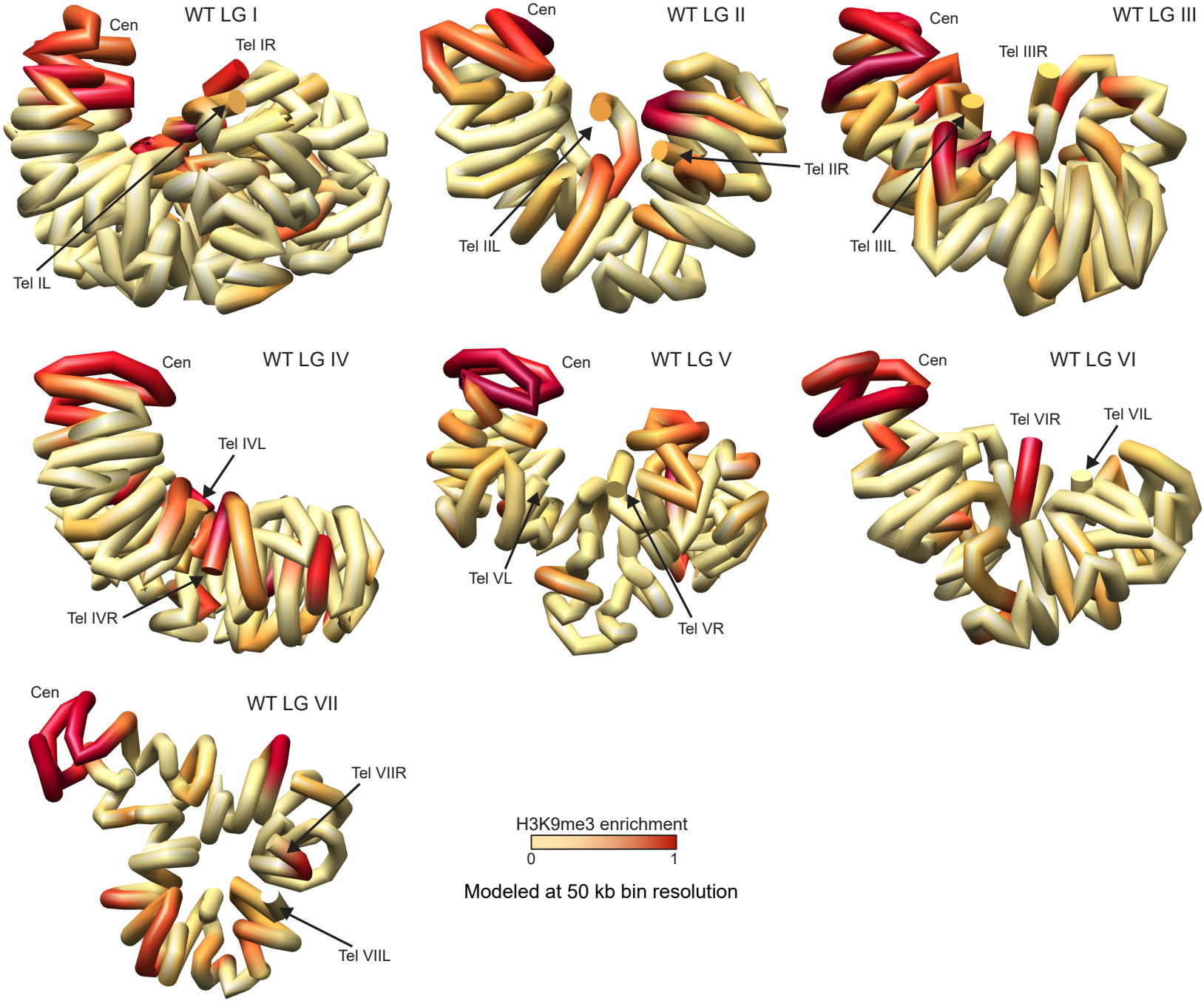
WT LG I
Cen
Tel IR
Tel IL
WT LG II
Cen
Tel IIR
Tel IIL
WT LG III
Cen
Tel IIIR
Tel IIIL
WT LG IV
Cen
Tel IVL
Tel IVR
WT LG V
Cen
Tel VL
Tel VR
WT LG VI
Cen
Tel VIR
Tel VIL
WT LG VII
Cen
Tel VIIR
Tel VIIL
H3K9me3 enrichment
0
1
Modeled at 50 kb bin resolution

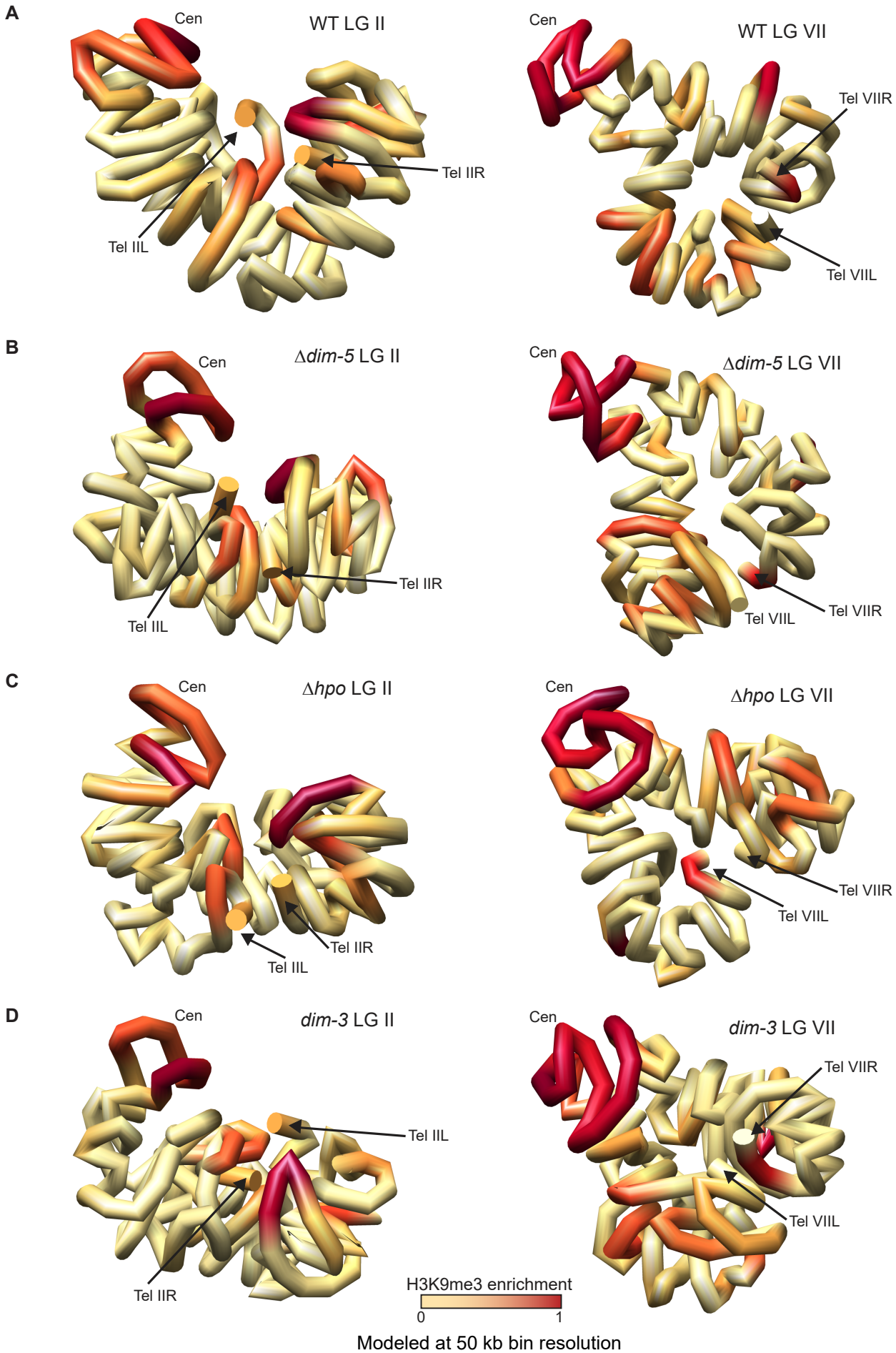
A
Cen
WT LG II
Tel IIR
Tel IIL
Cen
WT LG VII
Tel VIIR
Tel VIIL
B
Cen
Δdim-5 LG II
Tel IIR
Tel IIL
Cen
Δdim-5 LG VII
Tel VIIL
Tel VIIR
C
Cen
Δhpo LG II
Tel IIR
Tel IIL
Cen
Δhpo LG VII
Tel VIIR
Tel VIIL
D
Cen
dim-3 LG II
Tel IIL
Tel IIR
Cen
dim-3 LG VII
Tel VIIR
Tel VIIL
H3K9me3 enrichment
0
1
Modeled at 50 kb bin resolution